
INSPECT: A Multimodal Dataset for Pulmonary Embolism Diagnosis and Prognosis

Shih-Cheng Huang*
Stanford University
mschuang@stanford.edu

Zepeng Huo*
Stanford University
zphuo@stanford.edu

Ethan Steinberg*
Stanford University
ethanid@stanford.edu

Chia-Chun Chiang
Mayo Clinic
chiang.chia-chun@mayo.edu

Matthew P. Lungren
Microsoft
mlungren@microsoft.com

Curtis P. Langlotz
Stanford University
langlotz@stanford.edu

Serena Yeung
Stanford University
syyeung@stanford.edu

Nigam H. Shah
Clinical Excellence Research Center
Stanford University
Technology and Digital Solutions
Stanford Healthcare
nigam@stanford.edu

Jason A. Fries
Stanford University
jfries@stanford.edu

Abstract

Synthesizing information from multiple data sources plays a crucial role in the practice of modern medicine. Current applications of artificial intelligence in medicine often focus on single-modality data due to a lack of publicly available, multimodal medical datasets. To address this limitation, we introduce INSPECT, which contains de-identified longitudinal records from a large cohort of patients at risk for pulmonary embolism (PE), along with ground truth labels for multiple outcomes. INSPECT contains data from 19,402 patients, including CT images, radiology report impression sections, and structured electronic health record (EHR) data (i.e. demographics, diagnoses, procedures, vitals, and medications). Using INSPECT, we develop and release a benchmark for evaluating several baseline modeling approaches on a variety of important PE related tasks. We evaluate image-only, EHR-only, and multimodal fusion models. Trained models and the de-identified dataset are made available for non-commercial use under a data use agreement. To the best of our knowledge, INSPECT is the largest multimodal dataset integrating 3D medical imaging and EHR for reproducible methods evaluation and research¹.

1 Introduction

The practice of modern medicine is inherently multimodal, where synthesizing information from multiple data sources is essential for *diagnosis* (identifying which condition a patient currently has) and *prognosis* (predicting the likely course or outcome of a disease). Physicians routinely analyze patients' current symptoms and past medical history by examining imaging modalities such as X-rays and reviewing electronic health record (EHR) data to diagnose conditions, monitor disease progression, and tailor treatment plans [40, 10]. Artificial intelligence (AI) models capable of emulating the multimodal approach of contemporary medicine hold significant promise for enhancing the efficiency and accuracy of medical diagnosis, prognosis, and treatment planning.

¹<https://inspect.stanford.edu>

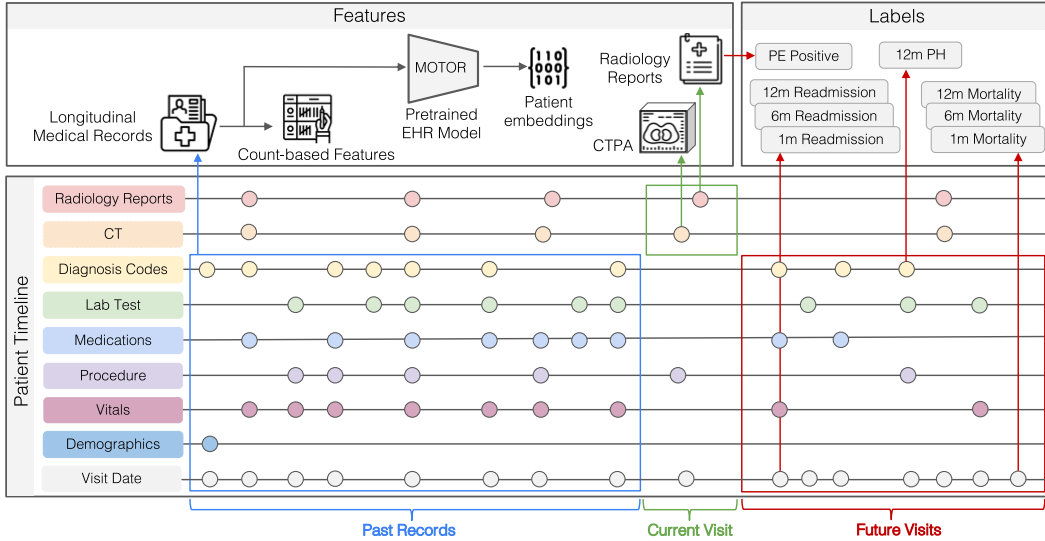


Figure 1: The INSPECT dataset comprises 19,402 patients’ structured longitudinal EHRs, which includes diagnosis/procedure codes, labs, medications, vitals, and demographics, as well as 23,248 CT-scans paired with their corresponding radiology report impression section. We curated PE diagnostic and prognostic labels based on these radiology reports and subsequent visit data.

Recent advancements in *multimodal fusion* strategies have enabled medical AI models to process a wide variety of input modalities, including complimentary imaging [49, 6], EHRs [24], clinical reports [65], genomics [53], and improve model performance. Many prior works have applied multimodal fusion in medical imaging [25, 20, 14], but prognostic tasks have garnered less attention compared to diagnostic ones, primarily due to challenges in obtaining longitudinal data. For instance, prognostic tasks such as predicting 6-month mortality require future data to assign labels and involve inherently longer time horizons than diagnostic tasks. Existing medical imaging datasets are small in size [67], do not include diverse data modalities [44], or have few diagnosis/prognosis labels [38]. Addressing these limitations via new multimodal imaging datasets is essential to further advance AI-driven diagnostic and prognostic tools.

In response to these challenges, we present INSPECT (**I**ntegrating **N**umerous **S**ources for **P**rognostic **E**valuation of **C**linical **T**imelines), a multimodal dataset of patients at risk for pulmonary embolism (PE). In clinical settings, multimodal data are vital for identifying long-term complications of PE. Specifically, imaging markers from CT pulmonary angiograms (CTPA) improve prediction accuracy for adverse events [52] and combining CTPA data with EHR data increases the effectiveness of automated PE diagnosis [25]. However, the potential benefits of multimodal methods for prognosis in PE have not been fully explored, mainly due to the lack of extensive multimodal datasets with outcome labels. With INSPECT, we aim to aid in the development of new methods for multimodal fusion, tapping into both known and yet-to-be-discovered biomarkers for PE outcome prediction.

INSPECT is made available under a Data Use Agreement (DUA) for non-commercial research use. Our contributions are summarized as follows:

1. A large-scale, multimodal medical dataset. INSPECT contains 23,248 CTPA studies from 19,402 patients, each including: (1) high-resolution CT images (3D volumetric pixel data) with (2) paired radiology report impression sections, (3) structured longitudinal electronic health record (EHR) data and (4) clinically relevant labels, including diagnostic and prognostic labels. Each patient’s longitudinal EHR provides a timeline of medical codes, demographics, medications, labs, vitals, procedures, and diagnoses. To our knowledge, this is the first dataset that combines 3D medical imaging with both radiology reports and longitudinal EHRs.

2. A benchmark for PE diagnosis and prognosis. We establish a benchmark for diagnosing and forecasting outcomes of pulmonary embolism through eight clinically important tasks. We assess various imaging and EHR modeling techniques, including individual models using only medical images or EHR data and combined models that use both modalities. All software and trained models used in our benchmark are available open source.

Dataset	Modalities			Counts		Curated Task Labels	
	Images	Reports	EHR	Patients	Studies	Diagnostic	Prognostic
UK Biobank [7]	MRI, DXA, Ultrasound	✗	*	100,000	many	✗	✗
Open-I [16]	Chest X-ray	✓	✗	3,955	7,466	✗	✗
CheXpert [30]	Chest X-ray	✗	✗	65,240	224,316	14	✗
MIMIC-CXR [32]	Chest X-ray	✓	✓	65,379	227,835	14	✗
RSPECT [11]	CT	✗	✗	12,195	12,195	13	✗
RadFusion [68]	CT	✗	*	1,794	1,837	1	✗
INSPECT (Ours)	CT	✓	✓	19,402	23,248	1	3

Table 1: INSPECT vs. existing multimodal medical image datasets (* denotes partial availability).

2 Related Work

2.1 Medical AI for Pulmonary Embolism

Pulmonary embolism (PE) is a serious medical condition responsible for nearly 300,000 hospital admissions and approximately 180,000 fatalities each year in the United States [21]. Despite the high mortality rate associated with PE, research suggests that timely identification and commencement of appropriate treatment strategies can markedly lower both morbidity and mortality rates [41, 42]. A definitive PE diagnosis is achieved through computed tomography pulmonary angiography (CTPA) [39]; however, patients diagnosed with PE typically endure more than six days of diagnostic delay, and a quarter of these patients are misdiagnosed during their initial visit [1, 19]. Estimating long-term patient outcomes is a critical factor that can aid hospitals in efficiently allocating resources and developing an optimal patient care plan. Current practice primarily depends on rudimentary metrics such as the Pulmonary Embolism Severity Index (PESI) scoring system [54], which only considers a limited set of clinical variables.

Many studies have investigated the automation of PE detection and patient triage to alleviate the burden on radiologists [23, 25, 62, 48, 27, 58, 28]. Most of these studies do not incorporate EHR data into models, even though these records contain crucial patient history and demographic details that are essential for accurate clinical interpretation of medical images [24]. Moreover, there is a notable lack of models focused on predicting long-term outcomes for PE patients [4], largely due to the lack of publicly accessible datasets containing these labels. Hence, further research and model development that includes long-term outcome prediction and comprehensive patient EHRs have the potential to significantly improve PE detection and management.

2.2 Multimodal Fusion for Medical Image Applications

Incorporating clinical context is critical for accurate diagnostic interpretation of medical images. Limiting a radiologist’s access to patient EHR data significantly reduces their diagnostic accuracy. Research has consistently highlighted the importance of clinical history, vitals, and lab data in accurately interpreting medical images [40, 10, 13, 12, 34]. Similarly, medical imaging models that use patient EHR data have improved accuracy and clinical relevance [24, 3, 22]. Many studies have shown the benefits of adding clinical context rather than relying solely on imaging data [64, 36, 66, 43, 26, 59, 47, 56, 29]. Nevertheless, a majority of these studies rely on a restricted subset of clinical features, primarily due to the dearth of large-scale, multimodal medical datasets. Consequently, these studies are unable to take full advantage of multimodal data fusion, highlighting the need for more comprehensive research approaches and dataset collection efforts.

2.3 Multimodal Datasets

Publicly available medical datasets continue to drive significant advances in medical AI research [30, 33, 68, 11]. However, very few currently available datasets include multiple modalities, are large scale, and have extensive labeled data, particularly in medical domains leveraging 3D medical images (Table 1). The limitations in data availability primarily stem from the inherent challenges associated with the release of medical data. Publicly sharing patient data requires rigorous review processes to safeguard sensitive patient information from inadvertent exposure. Furthermore, the process of labeling is often a labor-intensive and expensive endeavor. The additional challenge of managing the substantial size of 3D medical data further compounds these issues.

Among previous contributions, the MIMIC dataset [33, 31, 32] stands out as a large-scale work incorporating multiple modalities, with linkages provided with 2D chest x-rays. However, MIMIC lacks 3D medical imaging. The UK Biobank contains a variety of medical imaging modalities (e.g. MRIs, ultrasounds) combined with longitudinal medical record data [8]. However, UK Biobank imaging studies are collected prospectively, creating challenges in studying specific medical conditions, and do include corresponding radiology reports [46].

Radfusion [68] combines EHR summary statistics with 3D CT scans. However, Radfusion is a small-scale dataset that does not include longitudinal structured EHR data (i.e., timestamped vitals, labs, procedures, diagnoses, etc.), radiology reports, and outcome labels. Lastly, the RSNA-STR PE CT (RSPECT) dataset [11] contains 12,195 CTPA studies, but provides only a single modality, a single case per patient, and does not include prognosis labels. Our study addresses these gaps by introducing a large-scale dataset extracted from 23,248 PE cases and offers multiple modalities and labels, promising to enrich future research in this space.

3 Cohort Definition & Dataset Composition

Our study, approved by the Stanford Institutional Review Board (Appendix A), identified 155,950 cases involving CT pulmonary angiography at Stanford Medicine (2000-2021) using the STANford Medicine Research Data Repository (STARR) [9]. Our cohort of CTPA cases was defined through a protocol involving random sampling, data cleaning, and inclusion criteria adherence, resulting in a final cohort of 23,248 CTPA cases for 19,402 distinct patients (see Appendix B for details). For each case, we obtained the DICOM (Digital Imaging and Communications in Medicine) files for the CT scans, the corresponding radiology reports for those scans, and structured EHR data from STARR. Each of these was then processed for analysis and de-identification. We also defined canonical training, validation, and test splits that comprise 80%, 5%, and 15% of the dataset, respectively. We defined splits based on patient IDs, such that each patient only appears in one split.

Demographics Statistics								
Attributes		All	Train		Val		Test	
	Cases	23,248	18,945	(81.5%)	1,089	(4.7%)	3,214	(13.8%)
	Patients	19,402	15,789	(81.4%)	913	(4.7%)	2,700	(13.9%)
Overlapping Studies	RSPECT [11]	579	579	(2.5%)	0	(0.00%)	0	(0.00%)
	RadFusion [68]	772	772	(3.3%)	0	(0.00%)	0	(0.00%)
Gender	Female	10,733	8,695	(55.1%)	517	(56.6%)	1,521	(56.3%)
	Male	8,666	7,091	(44.9%)	396	(43.4%)	1,179	(43.7%)
	Unknown	3	3	(0.00%)	0	(0.00%)	0	(0.00%)
Age	0-18	0	0	(0.0%)	0	(0.0%)	0	(0.0%)
	18-39	2,912	2,380	(15.1%)	143	(15.7%)	389	(14.4%)
	39-69	9,974	8,135	(51.5%)	465	(50.9%)	1,374	(50.9%)
	69-89	5,859	4,740	(30.0%)	268	(29.4%)	851	(31.5%)
	>89	657	534	(3.4%)	37	(4.1%)	86	(3.2%)
Race	White	10,704	8,722	(55.2%)	502	(55.0%)	1,480	(54.8%)
	Asian	2,976	2,378	(15.1%)	152	(16.6%)	446	(16.5%)
	Black	1,103	910	(5.8%)	37	(4.1%)	156	(5.8%)
	Native	415	337	(2.1%)	22	(2.4%)	56	(2.1%)
	Unknown	4,204	3,442	(21.8%)	200	(21.9%)	562	(20.8%)
Ethnicity	Not Hispanic	15,628	12,709	(80.5%)	729	(79.8%)	2,190	(81.1%)
	Hispanic	3,018	2,448	(15.5%)	158	(17.3%)	412	(15.3%)
	Unknown	756	632	(4.0%)	26	(2.8%)	98	(3.6%)

Table 2: Demographics statistics of the INSPECT dataset. Demographic percentages are marked in light blue. The prevalence of overlapping cases between RSPECT and Radfusion with INSPECT is also indicated. No training data from RSPECT and Radfusion are included in our validation/test sets.

Table Type	Whole Cohort		Per Patient		
	# Records	Percentage	Median	Min	Max
Measurement	183,820,762	(81.5 %)	3,783	0	500,368
Drug exposure	17,288,279	(7.67 %)	271	0	118,228
Procedure occurrence	8,614,273	(3.82 %)	190	1	35,926
Condition occurrence	8,320,211	(3.69 %)	148	0	27,480
Visit occurrence	5,865,211	(2.60 %)	126	1	16,336
Visit detail	1,355,691	(0.60 %)	23	0	4,840
Device exposure	88,010	(0.03 %)	1	0	682
Person	87,158	(0.03 %)	4	1	48
Death	4,410	(0.001 %)	0	0	13
Total	225,444,005	(100 %)	5,080	7	741,873

Table 3: Summary statistics of the longitudinal EHR data included in INSPECT.

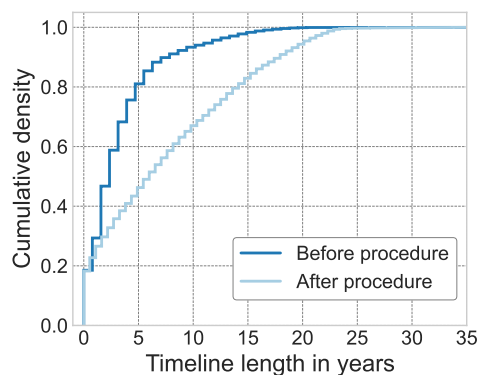


Figure 2: The cumulative probability distribution of EHR timeline lengths before and after CTPA.

Summary statistics of the demographic characteristics of our final cohort are available in Table 2. A small subset of the studies in our dataset has already been published as part of the RSPECT [11] and Radfusion [68] datasets. To maintain the integrity of our model testing process, we have ensured that no training data from the RSPECT and Radfusion datasets are included in our validation and test set. Similarly, we have also ensured that none of the validation and test data from the RSPECT and Radfusion datasets appear in our training set. This guarantees a clear separation between training and testing data, essential for unbiased model evaluation. We have indicated the prevalence of overlapping cases in Table 2. Based on this cohort, we release the following as the INSPECT dataset:

- **CTPA:** the imaging slices for the CTPAs in our cohort in DICOM format.
- **DICOM Headers:** a subset of the DICOM headers from the original DICOM file, including Patient ID, study date, instance order in the series, patient position, pixel spacing, rescale slope, rescale intercept, imaging machine manufacturer, and slice thickness. We made sure that patient ID and study date were anonymized to ensure patient privacy.
- **Radiology Report Impressions:** the impression section of the corresponding radiologist report for all the CTPAs in our cohort.
- **Structured Data From EHRs:** de-identified structured data from longitudinal EHR records for each patient in our cohort, including diagnoses, procedures, lab results, medications, and demographics. Each data element consists of a timestamp for when the event occurred, a code signifying the type of event, and optionally, a value (for lab results and vitals). All clinical events and known encounters with Stanford Health Care are included. A distribution showing the event frequency is in Table 3.

A detailed description of the formatting, hosting, and licensing details of INSPECT is in AppendixC.

4 Benchmark

In addition to the INSPECT dataset, we developed a benchmark for evaluating predictive models on our cohort. The code for this benchmark is included in the supplement under an open-source license.

4.1 Data Processing

CTPA Each CTPA exam is preprocessed by extracting the pixel data from the original DICOM format. We linearly transform the extracted pixel data in Hounsfield Units (HU) using the rescale slope and intercept recorded in the DICOM file. Specifically, each image x is processed with $x = x * s + b$, where s is the rescale slope and b is the rescale intercept.

Radiologist Reports All CTPA exams are accompanied by a radiology report that contains a summary of the patient’s medical history and detailed descriptions of the medical conditions observed by the radiologist. Using a rule-based system, we process these reports by extracting the impression section - a summary of the most important findings and possible causes. In addition, We deidentify the impression section by replacing dates and names with deidentified keywords.

Electronic Health Records Our source EHR records are stored in the OMOP schema [57]. They contain longitudinal EHR for patients seen at Stanford Health Care (comprised of an adult hospital and outpatient clinics) and Stanford Children’s Hospital. Each record contains demographic information (age, sex, ethnicity), and coded clinical information (diagnosis codes, lab test orders and results, medication orders, procedures, and visits). The cumulative probability distribution of patient EHR timeline lengths before and after CTPA procedures is shown in Figure 2. We processed the EHR records using the FEMR (<https://github.com/som-shahlab/femr>) software package and exported data for release in FEMR’s CSV format. In order to enable release, we anonymize INSPECT by introducing random time shifts for every patient, removing structured patient identifiers, and removing all unstructured text.

O	T	L	All	Train		Val		Test	
PE	N/A	pos.	4,689	3,924	(20.7 %)	188	(17.3 %)	577	(18.0 %)
		neg.	18,559	15,021	(79.3 %)	901	(82.7 %)	2,637	(82.0 %)
Mort	1 m	pos.	1,200	986	(5.2 %)	54	(5.0 %)	160	(5.0 %)
		neg.	20,803	16,930	(89.4 %)	991	(91.0 %)	2,882	(89.7 %)
		cen.	1,245	1,029	(5.4 %)	44	(4.0 %)	172	(5.4 %)
	6 m	pos.	2,389	1,963	(10.4 %)	103	(9.5 %)	323	(10.0 %)
		neg.	18,552	15,075	(79.6 %)	900	(82.6 %)	2,577	(80.2 %)
		cen.	2,307	1,907	(10.1 %)	86	(7.9 %)	314	(9.8 %)
	12 m	pos.	2,916	2,390	(12.6 %)	129	(11.8 %)	397	(12.4 %)
		neg.	17,157	13,936	(73.6 %)	829	(76.1 %)	2,392	(74.4 %)
		cen.	3,175	2,619	(13.8 %)	131	(12.0 %)	425	(13.2 %)
Re-ad	1 m	pos.	857	695	(3.7 %)	38	(3.5 %)	124	(3.9 %)
		neg.	20,774	16,898	(89.2 %)	997	(91.6 %)	2,879	(89.6 %)
		cen.	1,617	1,352	(7.1 %)	54	(5.0 %)	211	(6.6 %)
	6 m	pos.	2,185	1,778	(9.4 %)	99	(9.1 %)	308	(9.6 %)
		neg.	17,953	14,585	(77.0 %)	878	(80.6 %)	2,490	(77.5 %)
		cen.	3,110	2,582	(13.6 %)	112	(10.3 %)	416	(12.9 %)
	12 m	pos.	2,826	2,291	(12.1 %)	130	(11.9 %)	405	(12.6 %)
		neg.	16,253	13,201	(69.7 %)	794	(72.9 %)	2,258	(70.3 %)
		cen.	4,169	3,453	(18.2 %)	165	(15.2 %)	551	(17.1 %)
PH	12 m	pos.	2,726	2,242	(11.8 %)	124	(11.4 %)	360	(11.2 %)
		neg.	16,503	13,389	(70.7 %)	804	(73.8 %)	2,310	(71.9 %)
		cen.	4,019	3,314	(17.5 %)	161	(14.8 %)	544	(16.9 %)

Table 4: Task statistics for INSPECT. **O**: Outcome. **T**: Time Horizon. **L**: Label Value, **PE**: Pulmonary Embolism, **Mort**: In-Hospital Mortality, **Re-ad**: Re-admission, **PH**: Pulmonary Hypertension.

4.2 Task Definitions

Formally, given a set of multi-variate features, $\mathbf{x}_1, \dots, \mathbf{x}_N$, which are encoded from the occurrences of the selected covariates in Table 3, which is a composite set of clinical events happening in continuous time steps t_1, \dots, t_N . The goal is to train a model to approach the posterior probability of predicting the future event t_{i+m} at a specific time horizon: $p[(t_{i+m}, y)|(t_i, \mathbf{x}_i)]$, where \mathbf{x}_i is an accumulative feature at time t_i that encodes information from features from all previous time steps $\mathbf{x}_i = f(\mathbf{x}_1, \dots, \mathbf{x}_{i-1})$ and $f(\cdot)$ is the EHR modality model to be learned. The time horizon m was a set of predefined periods in the future, and y was a binary variable to indicate the patient having the medical event at the timestamp t_{i+m} . When combined with other modalities, e.g. imaging modality features, we augmented the output of EHR model y_i^{EHR} at prediction time t_i with a late fusion:

$$\hat{y} := \mathbf{w} \begin{bmatrix} y^{\text{EHR}} \\ \vdots \\ y^{\text{image}} \end{bmatrix}, \quad (1)$$

where the fusion weights \mathbf{w} were learned from the validation set.

In the following sections, we elaborate on the precise definition for each task and how the corresponding labels are generated. Table 4 contains various statistics on the labels for each task.

4.2.1 Diagnostic Tasks

Pulmonary Embolism (PE): We construct a pulmonary embolism diagnostic task that classifies whether pulmonary embolism is diagnosed based on the patient’s CT scan. Labels are generated by applying an NLP model to the *impression* section of the corresponding radiology report. Specifically, we first fine-tune a Clinical Longformer [45] model to predict pulmonary embolism diagnoses given the impression section of a text radiology report. Ground truth labels for the reports are manually collected by [5]. Subsequently, we apply the fine-tuned model to all the impression sections of all studies in our dataset to assign a pulmonary embolism diagnosis (or lack of diagnosis) to every patient in our cohort. Appendix D describes how this model was trained and how we validated its performance.

4.2.2 Prognostic Tasks

For the prognostic tasks, we attempt to predict whether or not a specific event will occur in the future within a specified time horizon for a given patient. To handle missing data, patients without a recorded prognosis event and those lacking data up to the time horizon are considered censored. These patients are excluded from both training and evaluation.

The event definitions are as follows:

- **Pulmonary Hypertension (PH):** A set of 29 International Classification of Diseases (ICD) codes to identify pulmonary hypertension.
- **In-Hospital Mortality:** We use the in-hospital mortality events provided by STARR-OMOP.
- **Re-admission:** We use the inpatient readmission events provided by STARR-OMOP.

Appendix D contains the set of ICD codes used for PH definition and outlines the methodology employed to validate this set of codes.

4.3 Baseline Models

We set up several common modeling approaches for each data type to serve as baselines, including image-only, EHR-only, and multimodal fusion models. The following are brief descriptions of each overall approach. The baseline model construction is shown in Figure 3. Full details, including hyperparameter tuning, can be found in Appendix F.

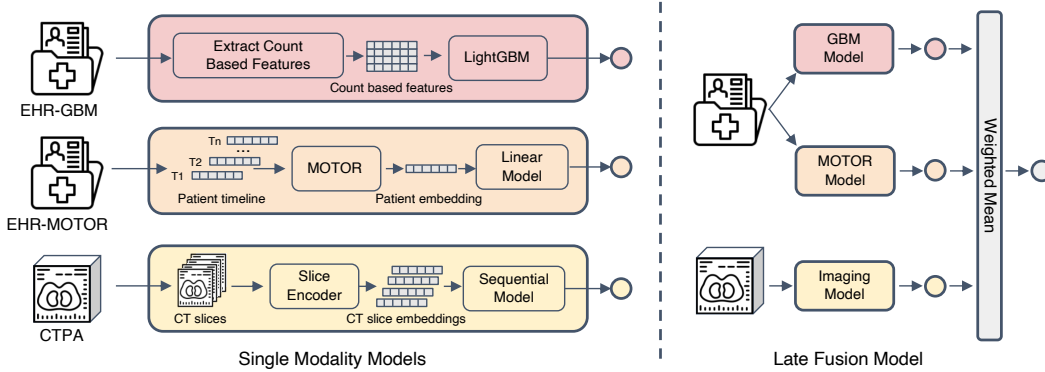


Figure 3: **Baseline Models.** We evaluate both single modality models and multi-modal late fusion models that incorporate data from both images and EHRs as baselines. For CT input, we use an LRCN (Long-term Recurrent Convolutional) model, while for structured EHR input, we employ MOTOR and gradient-boosted trees. Our multi-modal fusion baseline utilizes a late fusion approach, learning a weighted mean from each individual modality’s predicted probability.

4.3.1 Imaging

We resize all CTPA exams to 256 by 256 pixels. Following this, we refine the focus of each slice through center cropping, resulting in a 224 by 224 pixel matrix. Subsequently, we introduce three viewing windows to highlight particular structures. Each of these windows offers an optimal view for a specific medical perspective: the lung, pulmonary embolism, and mediastinum. We then stack the three view windows into three channels, giving us an array of 224x224x3 for each CT slice. Finally, we normalize each CTPA exam to be zero-centered using ImageNet mean and standard deviation.

Figure 3 illustrates the two-step process of our CTPA model, encompassing feature extraction and sequential modeling. First, we employ a pretrained image encoder for feature extraction, processing each CT slice into a latent representation. Subsequently, all extracted features from a given CT series are inputted into a sequence encoder for our final prediction. As a baseline, we leverage a ResNetV2 model pretrained on BigTransfer [37] and finetuned on the RSPECT dataset [11] as slice encoder. For a sequence encoder, we use either an LSTM, GRU, or Transformer model [17].

4.3.2 Structured EHRs

Gradient-boosted Trees

In order to build a gradient-boosted tree model, we first featurize our structured EHR data using a common count-featurization approach [60] that creates a matrix that counts the number of times each code appears in the EHR before the index date. We then train LightGBM [35] models on these count matrix features.

Structured EHR Foundation Model

To address the difficulty of training a deep learning model on small datasets, we adapt MOTOR [63], a foundation model that was pretrained on Stanford structured EHR data. MOTOR was pretrained using time-to-event tasks, making it well-aligned with our desired prognostic prediction tasks. We ensure that none of the patients in our validation or test set were used for pretraining. We then fit a linear probe (i.e., a linear layer and frozen MOTOR backbone) for all tasks.

4.3.3 Multimodal Fusion

We evaluate multimodal fusion strategies[24] to combine our three baseline models. Our fusion models (see Figure 3) aggregate prediction probabilities from individual models by taking a weighted mean of these probabilities of each single-modality model. The weights are trained by learning a logistic regression model on the validation set using individual model probabilities as features.

Input Modality			Diagnostic	Prognostic						
Image	EHR		PE	In-Hospital Mortality			Re-admission			PH
CT	M	G	(+)	1 m	6 m	12 m	1 m	6 m	12 m	12 m
✓	✓		<u>0.721</u>	0.794	0.755	0.748	0.549	0.515	0.525	0.661
			0.677	<u>0.923</u>	<u>0.901</u>	<u>0.892</u>	<u>0.773</u>	<u>0.779</u>	<u>0.767</u>	0.824
		✓	0.681	0.848	0.865	0.855	0.737	0.740	0.728	<u>0.828</u>
✓	✓		0.761	0.924	0.903	0.895	0.774	0.777	0.764	0.820
✓		✓	0.765	0.867	0.875	0.866	0.740	0.736	0.722	0.830
	✓	✓	0.699	0.922	0.903	0.892	0.782	0.786	0.774	0.849
✓	✓	✓	0.771	0.924	0.904	0.895	0.782	0.784	0.771	0.843

Table 5: The performance in AUROC for our different baseline modeling strategies, including various late fusions. **CT** is the CTPA based LRCN (Long-term Recurrent Convolutional Networks) model, **M** is the structured EHR based MOTOR model, and **G** is the structured EHR based gradient-boosted trees model. The best overall models are **bolded** and the best individual models are underlined.

5 Experiments And Results

To validate our dataset and provide some baselines, we perform experiments applying each of our three modeling strategies to each of our tasks. We also perform model fusion on each combination of individual models. Details on the computational resources used to run our experiments are in Appendix G. We also release the trained model weights learned in our experiments as part of our dataset, so our experiments can be reproduced (see Appendix C).

Table 5 contains the model performance in terms of AUROC for each of our approaches on each task. Confidence intervals can be found in Appendix H. When considering individual models, we find that the structured EHR models perform better on prognostic tasks while the CT model performs better on the diagnostic PE task. This is to be expected given that our source PE diagnoses are defined using CT scans, so the CT modality contains the information that most directly solves the diagnostic task.

We find that model fusion between the CT model and the structured EHR models helps improve performance on the diagnostic PE task but does not improve performance on the prognostic tasks. While prior work has identified imaging biomarkers related to chronic disease using CT chest imaging [51, 18], it is unclear if current deep learning models are able to take advantage of these signals. We also note that our image-only model does not match some state-of-the-art models’ performance [50] on predicting PE on a similar dataset, i.e. RSPECT [11]. We posit the difference might come from nuanced label definition, where our PE definition (shown in Appendix D) has incorporated subsegmental PE where the RSPECT dataset did not.

6 Discussion

Our work to develop INSPECT represents a significant step forward in multimodal, multi-label, multi-timeframe medical AI research, contributing a rich, large-scale dataset and benchmarks in the context of pulmonary embolism. INSPECT encompasses diverse modalities – high-quality CT images, radiology reports, and structured EHRs – enabling the development of benchmark predictive models for PE diagnosis and prognostication. To the best of our knowledge, we are the first to link longitudinal EHR data to 3D medical images and their paired radiology reports. This dataset provides opportunities for the community to derive additional diagnostic/prognostic labels (e.g. diagnosis codes, procedure codes, lab results, medications) for either model pretraining or downstream tasks.

Our preliminary findings suggest that the integration of medical imaging and structured EHRs improves performance in diagnosing PE. However, we also find that incorporating medical imaging for prognostic tasks does not improve predictive performance, especially on the important pulmonary hypertension prediction task. These results conflict with domain knowledge and medical literature, where it has been demonstrated that CT images contain information on some of the causes of pulmonary hypertension [2]. The lack of improved performance in our study suggests that there is untapped potential in our existing techniques, either in the fundamental imaging models or the

synthesis of the imaging model output with models trained using EHR data. By releasing INSPECT , we hope to enable the research community to explore this challenge.

6.1 Societal Implications

The process of releasing comprehensive patient timelines carries the inherent risk of exposing identifiable information. To mitigate this risk, we have adhered to the best practices for data anonymization in accordance with HIPAA compliance standards. Further, we have released all datasets and model weights under DUA, which is a standard procedure for medical data, thus ensuring controlled access to the data and models. However, it is important to note that using these data and/or model weights to provide medical advice and or make care decisions is beyond the intended scope of use for the INSPECT dataset and associated models. To emphasize this, we have specified in our DUA that INSPECT data and models are for research purposes only, not for clinical decision-making.

6.2 Limitations

Firstly, INSPECT only contains data from a single site (Stanford Health Care), and models trained on INSPECT may not generalize to other patient populations. Secondly, labels are assigned based on NLP output and source EHR data, not manual chart review, and thus may be inaccurate in some cases. However, we have taken several steps to mitigate this, as detailed in Appendix D. Finally, for each CTPA image, we release only the impression section of the corresponding radiology report as de-identification protocols preclude releasing the entire note. This limits some analyses and experiments that would require entire radiology reports, beyond the impression section.

7 Conclusion

There are two main contributions to this work. First, we present a large-scale medical dataset INSPECT with multiple modalities, comprising health records from 19,402 patients, complete with high-quality CT images, portions of accompanying radiology reports, and structured data from patient EHRs. Second, we use this dataset to create a benchmark for a variety of important pulmonary embolism related tasks, with included baseline models. In conclusion, this work has laid the foundation for future research into multimodal fusion strategies for integrating 3D medical imaging data and patient EHR data. By openly sharing INSPECT, we hope to ignite new advances in this critical area of healthcare.

Acknowledgments and Disclosure of Funding

Research reported in this publication was supported by the National Heart, Lung, And Blood Institute of the National Institutes of Health Awards R01HL155410 and R01HL144555, the National Library Of Medicine of the National Institutes of Health Award R01LM012966, and AIMI-HAI seed grant at Stanford University. We would also like to thank the Clinical Excellence Research Center (CERC) at Stanford for their support. The content is solely the responsibility of the authors and does not necessarily represent the official views of the National Institutes of Health.

References

- [1] José Luis Alonso-Martínez, FJ Annicchero Sánchez, and MA Urbieto Echezarreta. Delay and misdiagnosis in sub-massive and non-massive acute pulmonary embolism. *European journal of internal medicine*, 21(4):278–282, 2010.
- [2] M. Ascha, R. D. Renapurkar, and A. R. Tonelli. A review of imaging modalities in pulmonary hypertension. *Ann Thorac Med*, 12(2):61–73, 2017.
- [3] Muhammad Adeel Azam, Khan Bahadar Khan, Sana Salahuddin, Eid Rehman, Sajid Ali Khan, Muhammad Attique Khan, Seifedine Kadry, and Amir H Gandomi. A review on multimodal medical image fusion: Compendious analysis of medical modalities, multimodal databases, fusion techniques and quality metrics. *Computers in biology and medicine*, 144:105253, 2022.
- [4] Andreas Gunter Bach, Bettina-Maria Taute, Nansalmaa Baasai, Andreas Wienke, Hans Jonas Meyer, Dominik Schramm, and Alexey Surov. 30-day mortality in acute pulmonary embolism: prognostic value of clinical scores and anamnestic features. *PLoS one*, 11(2):e0148728, 2016.
- [5] Imon Banerjee, Yuan Ling, Matthew C Chen, Sadid A Hasan, Curtis P Langlotz, Nathaniel Moradzadeh, Brian Chapman, Timothy Amrhein, David Mong, Daniel L Rubin, et al. Comparative effectiveness of convolutional neural network (cnn) and recurrent neural network (rnn) architectures for radiology text report classification. *Artificial intelligence in medicine*, 97:79–88, 2019.
- [6] Gaurav Bhatnagar, QM Jonathan Wu, and Zheng Liu. A new contrast based multimodal medical image fusion framework. *Neurocomputing*, 157:143–152, 2015.
- [7] UK Biobank. About uk biobank, 2014.
- [8] Clare Bycroft, Colin Freeman, Desislava Petkova, Gavin Band, Lloyd T Elliott, Kevin Sharp, Allan Motyer, Damjan Vukcevic, Olivier Delaneau, Jared O’Connell, et al. The uk biobank resource with deep phenotyping and genomic data. *Nature*, 562(7726):203–209, 2018.
- [9] Alison Callahan, Euan Ashley, Somalee Datta, Priyamvada Desai, Todd A Ferris, Jason A Fries, Michael Halaas, Curtis P Langlotz, Sean Mackey, José D Posada, et al. The stanford medicine data science ecosystem for clinical and translational research. *JAMIA open*, 6(3):ooad054, 2023.
- [10] Mervyn D Cohen. Accuracy of information on imaging requisitions: does it matter? *Journal of the American College of Radiology*, 4(9):617–621, 2007.
- [11] Errol Colak, Felipe C Kitamura, Stephen B Hobbs, Carol C Wu, Matthew P Lungren, Luciano M Prevedello, Jayashree Kalpathy-Cramer, Robyn L Ball, George Shih, Anouk Stein, et al. The rsna pulmonary embolism ct dataset. *Radiology: Artificial Intelligence*, 3(2):e200254, 2021.
- [12] Nneka I Comfere, Margot S Peters, Sarah Jenkins, Kandace Lackore, Kathleen Yost, and Jon Tilburt. Dermatopathologists’ concerns and challenges with clinical information in the skin biopsy requisition form: a mixed-methods study. *Journal of cutaneous pathology*, 42(5):333–345, 2015.
- [13] Nneka I Comfere, Olayemi Sokumbi, Victor M Montori, Annie LeBlanc, Larry J Prokop, M Hassan Murad, and Jon C Tilburt. Provider-to-provider communication in dermatology and implications of missing clinical information in skin biopsy requisition forms: a systematic review. *International journal of dermatology*, 53(5):549–557, 2014.
- [14] Can Cui, Haichun Yang, Yaohong Wang, Shilin Zhao, Zuhayr Asad, Lori A Coburn, Keith T Wilson, Bennett Landman, and Yuankai Huo. Deep multi-modal fusion of image and non-image data in disease diagnosis and prognosis: a review. *Progress in Biomedical Engineering*, 2023.
- [15] Somalee Datta, Jose Posada, Garrick Olson, Wencheng Li, Ciaran O’Reilly, Deepa Balraj, Joseph Mesterhazy, Joseph Pallas, Priyamvada Desai, and Nigam Shah. A new paradigm for accelerating clinical data science at stanford medicine. *arXiv preprint arXiv:2003.10534*, 2020.
- [16] Dina Demner-Fushman, Marc D Kohli, Marc B Rosenman, Sonya E Shooshan, Laritza Rodriguez, Sameer Antani, George R Thoma, and Clement J McDonald. Preparing a collection of radiology examinations for distribution and retrieval. *Journal of the American Medical Informatics Association*, 23(2):304–310, 2016.
- [17] Alexey Dosovitskiy, Lucas Beyer, Alexander Kolesnikov, Dirk Weissenborn, Xiaohua Zhai, Thomas Unterthiner, Mostafa Dehghani, Matthias Minderer, Georg Heigold, Sylvain Gelly, et al. An image is worth 16x16 words: Transformers for image recognition at scale. *arXiv preprint arXiv:2010.11929*, 2020.

- [18] Akane Haruna, Shigeo Muro, Yasutaka Nakano, Tadashi Ohara, Yuma Hoshino, Emiko Ogawa, Toyohiro Hirai, Akio Niimi, Koichi Nishimura, Kazuo Chin, et al. Ct scan findings of emphysema predict mortality in copd. *Chest*, 138(3):635–640, 2010.
- [19] Janneke MT Hendriksen, Marleen Koster-van Ree, Marcus J Morgenstern, Ruud Oudega, Roger EG Schutgens, Karel GM Moons, and Geert-Jan Geersing. Clinical characteristics associated with diagnostic delay of pulmonary embolism in primary care: a retrospective observational study. *BMJ open*, 7(3):e012789, 2017.
- [20] Haithem Hermessi, Olfa Mourali, and Ezzeddine Zagrouba. Multimodal medical image fusion review: Theoretical background and recent advances. *Signal Processing*, 183:108036, 2021.
- [21] Kenneth T Horlander, David M Mannino, and Kenneth V Leeper. Pulmonary embolism mortality in the united states, 1979-1998: an analysis using multiple-cause mortality data. *Archives of internal medicine*, 163(14):1711–1717, 2003.
- [22] Bing Huang, Feng Yang, Mengxiao Yin, Xiaoying Mo, and Cheng Zhong. A review of multimodal medical image fusion techniques. *Computational and mathematical methods in medicine*, 2020, 2020.
- [23] Shih-Cheng Huang, Tanay Kothari, Imon Banerjee, Chris Chute, Robyn L Ball, Norah Borus, Andrew Huang, Bhavik N Patel, Pranav Rajpurkar, Jeremy Irvin, et al. Penet—a scalable deep-learning model for automated diagnosis of pulmonary embolism using volumetric ct imaging. *NPJ digital medicine*, 3(1):61, 2020.
- [24] Shih-Cheng Huang, Anuj Pareek, Saeed Seyyedi, Imon Banerjee, and Matthew P Lungren. Fusion of medical imaging and electronic health records using deep learning: a systematic review and implementation guidelines. *NPJ digital medicine*, 3(1):136, 2020.
- [25] Shih-Cheng Huang, Anuj Pareek, Roham Zamanian, Imon Banerjee, and Matthew P Lungren. Multimodal fusion with deep neural networks for leveraging ct imaging and electronic health record: a case-study in pulmonary embolism detection. *Scientific reports*, 10(1):22147, 2020.
- [26] Shih-Cheng Huang, Liyue Shen, Matthew P Lungren, and Serena Yeung. Gloria: A multimodal global-local representation learning framework for label-efficient medical image recognition. In *Proceedings of the IEEE/CVF International Conference on Computer Vision*, pages 3942–3951, 2021.
- [27] Heidi Huhtanen, Mikko Nyman, Tarek Mohsen, Arho Virkki, Antti Karlsson, and Jussi Hirvonen. Automated detection of pulmonary embolism from ct-angiograms using deep learning. *BMC Medical Imaging*, 22(1):43, 2022.
- [28] Andetta R Hunsaker. Deep learning and risk assessment in acute pulmonary embolism, 2022.
- [29] Seung Hyup Hyun, Mi Sun Ahn, Young Wha Koh, and Su Jin Lee. A machine-learning approach using pet-based radiomics to predict the histological subtypes of lung cancer. *Clinical nuclear medicine*, 44(12):956–960, 2019.
- [30] Jeremy Irvin, Pranav Rajpurkar, Michael Ko, Yifan Yu, Silvana Ciurea-Ilcus, Chris Chute, Henrik Marklund, Behzad Haghgoo, Robyn L. Ball, Katie S. Shpanskaya, Jayne Seekins, David A. Mong, Safwan S. Halabi, Jesse K. Sandberg, Ricky Jones, David B. Larson, Curtis P. Langlotz, Bhavik N. Patel, Matthew P. Lungren, and Andrew Y. Ng. Chexpert: A large chest radiograph dataset with uncertainty labels and expert comparison. *CoRR*, abs/1901.07031, 2019.
- [31] Alistair Johnson, Lucas Bulgarelli, Tom Pollard, Leo Anthony Celi, Roger Mark, and S Horng IV. Mimic-iv-ed. *PhysioNet*, 2021.
- [32] Alistair EW Johnson, Tom J Pollard, Nathaniel R Greenbaum, Matthew P Lungren, Chih-ying Deng, Yifan Peng, Zhiyong Lu, Roger G Mark, Seth J Berkowitz, and Steven Horng. Mimic-cxr-jpg, a large publicly available database of labeled chest radiographs. *arXiv preprint arXiv:1901.07042*, 2019.
- [33] Alistair EW Johnson, Tom J Pollard, Lu Shen, Li-wei H Lehman, Mengling Feng, Mohammad Ghassemi, Benjamin Moody, Peter Szolovits, Leo Anthony Celi, and Roger G Mark. Mimic-iii, a freely accessible critical care database. *Scientific data*, 3(1):1–9, 2016.
- [34] Jost B Jonas, Tin Aung, Rupert R Bourne, Alain M Bron, Robert Ritch, and Songhomitra Panda-Jonas. Glaucoma—authors’ reply. *The Lancet*, 391(10122):740, 2018.
- [35] Guolin Ke, Qi Meng, Thomas Finley, Taifeng Wang, Wei Chen, Weidong Ma, Qiwei Ye, and Tie-Yan Liu. Lightgbm: A highly efficient gradient boosting decision tree. *Advances in neural information processing systems*, 30, 2017.

- [36] P Kharazmi, S Kalia, H Lui, ZJ Wang, and TK Lee. A feature fusion system for basal cell carcinoma detection through data-driven feature learning and patient profile. *Skin research and technology*, 24(2):256–264, 2018.
- [37] Alexander Kolesnikov, Lucas Beyer, Xiaohua Zhai, Joan Puigcerver, Jessica Yung, Sylvain Gelly, and Neil Houlsby. Big transfer (bit): General visual representation learning. In *Computer Vision—ECCV 2020: 16th European Conference, Glasgow, UK, August 23–28, 2020, Proceedings, Part V 16*, pages 491–507. Springer, 2020.
- [38] Ajith AK Kumar. Mortality prediction in the icu: The daunting task of predicting the unpredictable. *Indian Journal of Critical Care Medicine: Peer-reviewed, Official Publication of Indian Society of Critical Care Medicine*, 26(1):13, 2022.
- [39] Grégoire Le Gal and Henri Bounameaux. Diagnosing pulmonary embolism: running after the decreasing prevalence of cases among suspected patients. *Journal of thrombosis and haemostasis*, 2(8):1244–1246, 2004.
- [40] Adones Leslie, AJ Jones, and PR Goddard. The influence of clinical information on the reporting of ct by radiologists. *The British journal of radiology*, 73(874):1052–1055, 2000.
- [41] Ann N Leung, Todd M Bull, Roman Jaeschke, Charles J Lockwood, Phillip M Boiselle, Lynne M Hurwitz, Andra H James, Laurence B McCullough, Yusuf Menda, Michael J Paidas, et al. An official american thoracic society/society of thoracic radiology clinical practice guideline: evaluation of suspected pulmonary embolism in pregnancy. *American journal of respiratory and critical care medicine*, 184(10):1200–1208, 2011.
- [42] Ann N Leung, Todd M Bull, Roman Jaeschke, Charles J Lockwood, Phillip M Boiselle, Lynne M Hurwitz, Andra H James, Laurence B McCullough, Yusuf Menda, Michael J Paidas, et al. American thoracic society documents: an official american thoracic society/society of thoracic radiology clinical practice guideline—evaluation of suspected pulmonary embolism in pregnancy. *Radiology*, 262(2):635–646, 2012.
- [43] Hongming Li and Yong Fan. Early prediction of alzheimer’s disease dementia based on baseline hippocampal mri and 1-year follow-up cognitive measures using deep recurrent neural networks. In *2019 IEEE 16th International Symposium on Biomedical Imaging (ISBI 2019)*, pages 368–371. IEEE, 2019.
- [44] Yikuan Li, Shishir Rao, José Roberto Ayala Solares, Abdelaali Hassaine, Rema Ramakrishnan, Dexter Canoy, Yajie Zhu, Kazem Rahimi, and Gholamreza Salimi-Khorshidi. Behrt: transformer for electronic health records. *Scientific reports*, 10(1):1–12, 2020.
- [45] Yikuan Li, Ramsey M Wehbe, Faraz S Ahmad, Hanyin Wang, and Yuan Luo. Clinical-longformer and clinical-bigbird: Transformers for long clinical sequences. *arXiv preprint arXiv:2201.11838*, 2022.
- [46] Thomas J Littlejohns, Jo Holliday, Lorna M Gibson, Steve Garratt, Niels Oesingmann, Fidel Alfaró-Almagro, Jimmy D Bell, Chris Boulwood, Rory Collins, Megan C Conroy, et al. The uk biobank imaging enhancement of 100,000 participants: rationale, data collection, management and future directions. *Nature communications*, 11(1):2624, 2020.
- [47] Ming-Qian LIU. Bone age assessment model based on multi-dimensional feature fusion using deep learning. *Academic journal of second military medical university*, pages 909–916, 2018.
- [48] Weifang Liu, Min Liu, Xiaojuan Guo, Peiyao Zhang, Ling Zhang, Rongguo Zhang, Han Kang, Zhenguo Zhai, Xincan Tao, Jun Wan, et al. Evaluation of acute pulmonary embolism and clot burden on ctpa with deep learning. *European radiology*, 30:3567–3575, 2020.
- [49] Zhaodong Liu, Hongpeng Yin, Yi Chai, and Simon X Yang. A novel approach for multimodal medical image fusion. *Expert systems with applications*, 41(16):7425–7435, 2014.
- [50] Xiaotian Ma, Emma C Ferguson, Xiaoqian Jiang, Sean I Savitz, and Shayan Shams. A multitask deep learning approach for pulmonary embolism detection and identification. *Scientific Reports*, 12(1):13087, 2022.
- [51] Ioana Mastora, Martine Remy-Jardin, Pascal Masson, Eric Galland, Valérie Delannoy, Jean-Jacques Bauchart, and Jacques Remy. Severity of acute pulmonary embolism: evaluation of a new spiral ct angiographic score in correlation with echocardiographic data. *European radiology*, 13:29–35, 2003.
- [52] Felix G Meinel, John W Nance Jr, U Joseph Schoepf, Verena S Hoffmann, Kolja M Thierfelder, Philip Costello, Samuel Z Goldhaber, and Fabian Bamberg. Predictive value of computed tomography in acute pulmonary embolism: systematic review and meta-analysis. *The American journal of medicine*, 128(7):747–759, 2015.

- [53] Pooya Mobadersany, Safoora Yousefi, Mohamed Amgad, David A Gutman, Jill S Barnholtz-Sloan, José E Velázquez Vega, Daniel J Brat, and Lee AD Cooper. Predicting cancer outcomes from histology and genomics using convolutional networks. *Proceedings of the National Academy of Sciences*, 115(13):E2970–E2979, 2018.
- [54] Lisa Moores, Celia Zamarro, Vicente Gómez, Drahomir Aujesky, Leticia García, Rosa Nieto, Roger Yusen, and David Jiménez. Changes in pesi scores predict mortality in intermediate-risk patients with acute pulmonary embolism. *European respiratory journal*, 41(2):354–359, 2013.
- [55] D. nez, D. Aujesky, L. Moores, V. mez, J. L. Lobo, F. Uresandi, R. Otero, M. Monreal, A. Muriel, R. D. Yusen, M. Monreal, H. Decousus, P. Prandoni, B. Brenner, R. Barba, P. Di Micco, K. Rivron-Guillot, J. I. Arcelus, M. n, A. Blanco, M. Bonilla, T. Bueso, I. as, I. Casado, F. Conget, C. á, C. n, P. Gallego, F. a Bragado, R. Guijarro, E. Grau, M. Guil, J. rrez, L. ndez, D. nez, R. Lecumberri, J. M. n, M. Llado, J. L. Lobo, L. pez, A. Lorenzo, J. M. Luque, O. Madridano, A. Maestre, P. J. Marchena, A. n, J. J. n Villasclaras, R. Monte, F. J. z, M. D. Naufall, J. A. Nieto, M. Oribe, M. T. Orue, R. Otero, J. Portillo, R. al, C. Renzi, A. Riera-Mestre, V. Rosa, S. Rubio, A. Ruiz-Gamietea, J. C. Sahuquillo, A. L. Samperiz, R. nchez, J. F. oz Torrero, R. Sandoval, S. Soler, G. Tiberio, R. Tirado, J. A. í, C. Tolosa, I. Torres, J. Trujillo-Santos, F. Uresandi, M. s, V. s, R. Valle, B. Vasco, J. Vela, H. Boccalon, N. Falvo, P. Le Corvoisier, K. Rivron-Guillot, G. Barillari, M. Ciammaichella, F. Dalla Valle, R. Duce, A. Ferrari, S. Pasca, G. Piovacari, R. Poggio, P. Prandoni, R. Quintavalla, A. Rocci, L. Rota, A. Schenone, E. Tiraferri, and A. à. Simplification of the pulmonary embolism severity index for prognostication in patients with acute symptomatic pulmonary embolism. *Arch Intern Med*, 170(15):1383–1389, Aug 2010.
- [56] Dong Nie, Junfeng Lu, Han Zhang, Ehsan Adeli, Jun Wang, Zhengda Yu, LuYan Liu, Qian Wang, Jinsong Wu, and Dinggang Shen. Multi-channel 3d deep feature learning for survival time prediction of brain tumor patients using multi-modal neuroimages. *Scientific reports*, 9(1):1103, 2019.
- [57] OHDSI. Omop common data model. <https://ohdsi.github.io/CommonDataModel/index.html>, 2023. Accessed: 2023-06-07.
- [58] Ian Pan. Deep learning for pulmonary embolism detection: tackling the rsna 2020 ai challenge. *Radiology: Artificial Intelligence*, 3(5):e210068, 2021.
- [59] Shikha Purwar, Rajiv Kumar Tripathi, Ravi Ranjan, and Renu Saxena. Detection of microcytic hypochromia using cbc and blood film features extracted from convolution neural network by different classifiers. *Multimedia Tools and Applications*, 79:4573–4595, 2020.
- [60] Alvin Rajkomar, Eyal Oren, Kai Chen, Andrew M Dai, Nissan Hajaj, Michaela Hardt, Peter J Liu, Xiaobing Liu, Jake Marcus, Mimi Sun, et al. Scalable and accurate deep learning with electronic health records. *NPJ digital medicine*, 1(1):18, 2018.
- [61] Bob Segert. Athena. <https://athena.ohdsi.org/>, 2023. Accessed: 2023-8-16.
- [62] Shelly Soffer, Eyal Klang, Orit Shimon, Yiftach Barash, Noa Cahan, Hayit Greenspana, and Eli Konen. Deep learning for pulmonary embolism detection on computed tomography pulmonary angiogram: a systematic review and meta-analysis. *Scientific reports*, 11(1):15814, 2021.
- [63] Ethan Steinberg, Yizhe Xu, Jason Fries, and Nigam Shah. Self-supervised time-to-event modeling with structured medical records. *arXiv preprint arXiv:2301.03150*, 2023.
- [64] Kim-Han Thung, Pew-Thian Yap, and Dinggang Shen. Multi-stage diagnosis of alzheimer’s disease with incomplete multimodal data via multi-task deep learning. In *Deep Learning in Medical Image Analysis and Multimodal Learning for Clinical Decision Support: Third International Workshop, DLMIA 2017, and 7th International Workshop, ML-CDS 2017, Held in Conjunction with MICCAI 2017, Québec City, QC, Canada, September 14, Proceedings*, pages 160–168. Springer, 2017.
- [65] Xiaosong Wang, Yifan Peng, Le Lu, Zhiyong Lu, and Ronald M Summers. Tienet: Text-image embedding network for common thorax disease classification and reporting in chest x-rays. In *Proceedings of the IEEE conference on computer vision and pattern recognition*, pages 9049–9058, 2018.
- [66] Jordan Yap, William Yolland, and Philipp Tschandl. Multimodal skin lesion classification using deep learning. *Experimental dermatology*, 27(11):1261–1267, 2018.
- [67] Zhuo Zhi, Moe Elbadawi, Adam Daneshmend, Mine Orlu, Abdul Basit, Andreas Demosthenous, and Miguel Rodrigues. Multimodal diagnosis for pulmonary embolism from ehr data and ct images. In *2022 44th Annual International Conference of the IEEE Engineering in Medicine & Biology Society (EMBC)*, pages 2053–2057. IEEE, 2022.

- [68] Yuyin Zhou, Shih-Cheng Huang, Jason Alan Fries, Alaa Youssef, Timothy J Amrhein, Marcello Chang, Imon Banerjee, Daniel Rubin, Lei Xing, Nigam Shah, et al. Radfusion: Benchmarking performance and fairness for multimodal pulmonary embolism detection from ct and ehr. *arXiv preprint arXiv:2111.11665*, 2021.

A IRB Approval and Data De-identification

Release of INSPECT was approved by the Stanford University Institutional Review Board (IRB), given data privacy review via a standardized workflow conducted by the Center for Artificial Intelligence in Medicine and Imaging (AIMI) and the University Privacy Office. Our study was approved by the Stanford University Administrative Panel on Human Subjects Research, protocol #24883, and included a waiver of consent. All included patients from SHC signed a privacy notice, which informs them that their records may be used for research purposes given approval by the IRB.

All INSPECT data (CT scans, DICOM metadata, radiology impression sections, EHR timelines) are manually reviewed by AIMI to confirm any protected health information (PHI) is removed before public release. We de-identify each modality as follows:

EHR Timelines: All dates are anonymized by using per-patient time jittering. We apply the same date transformation procedure used by MIMIC-III, specifically: "*[d]ates were shifted into the future by a random offset for each individual patient in a consistent manner to preserve intervals, resulting in stays which occur sometime between the years 2100 and 2200*" [33]. We remove all patients >89 years of age. We further remove all unstructured text fields that do not map to controlled vocabularies (e.g., SNOMED, LOINC) to prevent PHI leakage. We use OHDSI Athena [61] ontologies to describe our data, which includes both public ontologies like ICD-10 as well as OHDSI specific ontologies such as Race/Gender. The full list of ontologies used is in Table 6..

Ontology
OMOP Extension
Medicare Specialty
CPT4
CVX
ICD9Proc
RxNorm
SNOMED
RxNorm Extension
Cancer Modifier
ICD10PCS
CMS Place of Service
Visit
Ethnicity
Gender
ICDO3
Race
LOINC
HCPCS

Table 6: OHDSI Athena ontologies used in our benchmark

CT Scans: Each CT scan slice is manually reviewed for PHI, with slices containing patient information removed from the CT scan.

Radiology Notes: Radiology notes are preprocessed to include only the impression section, i.e., the description of radiologist findings in the corresponding CT scan. Each note is processed to tag names, locations, dates, telephone numbers and other HIPAA protected identifiers such as MRNs and accession numbers. These tags are then replaced with anonymized placeholder text. All deidentified notes are then manually reviewed to remove any additional PHI.

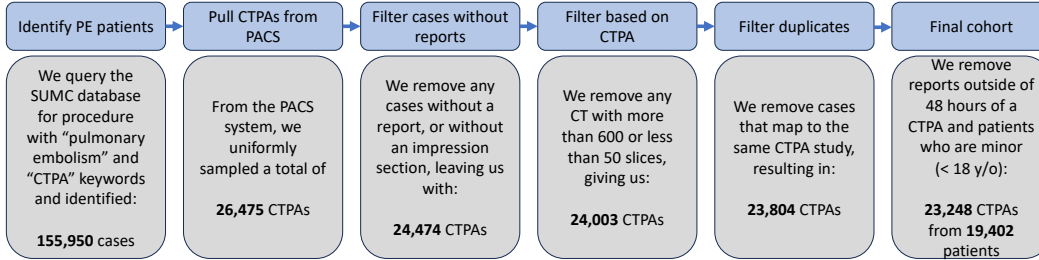


Figure 4: A flowchart of our cohort definition process.

B Cohort Definition

The flowchart of our cohort definition protocol is illustrated in Figure 4. With the approval from Stanford Institutional Review Board’s (IRB), we identified 155,950 cases with the CT pulmonary angiography (CTPA) procedure code from the STANford medicine Research data Repository (STARR) [15]. STARR data contains routinely collected EHR data from Stanford Health Care covering the time period of 2000 to 2021. We mapped each of these studies to their respective CTPA based on the procedure date. In instances where there was no exact match (1,296 cases) we extended the search to 10 days post-procedure date. From the mappable cases, we sampled uniformly at random 26,475 CT scans (chosen due to file storage constraints) and their corresponding radiology report.

The data cleaning phase followed, where we removed cases without a report or an impression section. This refinement process resulted in 24,474 cases for further analysis. We then selected the most relevant CTPA series per study by enforcing a slice thickness constraint between 1.0mm and 3.0mm, favoring thicker slice series. Additionally, CTs with over 600 or under 50 slices were removed from consideration. This filtering resulted in 24,003 studies. We further eliminated the test and validation data from RSNA and Radfusion in our training split and the training data thereof in our test and validation split. The patients who are minors (age < 18 years old) are removed due to privacy policy. The final selection phase involved eliminating cases with corrupted DICOMs and cases from the same patient that mapped to an identical study. The final result is a collection of 23,248 CTPA studies from a set of 19,402 unique patients.

C Dataset Documentation

C.1 Hosting, Access, License, and Long-Term Preservation

We share data and trained model weights under Data Use Agreement (DUA) for non-commercial, research use. The Stanford AIMI Center will host and ensure long-term preservation of all data. Complete licensing terms for dataset and models are provided below.

INSPECT is available at <https://stanfordaimi.azurewebsites.net/>. We provide a preview subset of the entire dataset for reviewers. Before public release, the entire dataset is currently undergoing manual review by the AIMI Center to ensure no leakage of patient identifying information.

As authors of the submitted dataset and corresponding manuscript, we hereby affirm that we take full responsibility for its contents. We ensure that this dataset and manuscript are original and that all data collection procedures were carried out ethically, respecting all relevant rights and regulations. We confirm that we have procured all necessary permissions for the use of the data included in the dataset, and that the data does not infringe upon any existing copyright, proprietary, or personal rights of others.

C.2 License Terms of Use

By registering for downloads from the INSPECT Dataset, you are agreeing to this Research Use Agreement, as well as to the Terms of Use of the Stanford University School of Medicine website as posted and updated periodically at <http://www.stanford.edu/site/terms/>.

Permission is granted to view and use the INSPECT Dataset without charge for personal, non-commercial research purposes only. Any commercial use, sale, or other monetization is prohibited.

Other than the rights granted herein, the Stanford University School of Medicine (“School of Medicine”) retains all rights, title, and interest in the INSPECT Dataset.

You may make a verbatim copy of the INSPECT Dataset for personal, non-commercial research use as permitted in this Research Use Agreement. If another user within your organization wishes to use the INSPECT Dataset, they must register as an individual user and comply with all the terms of this Research Use Agreement.

YOU MAY NOT DISTRIBUTE, PUBLISH, OR REPRODUCE A COPY of any portion or all of the INSPECT Dataset to others without specific prior written permission from the School of Medicine.

YOU MAY NOT SHARE THE DOWNLOAD LINK to the INSPECT Dataset to others. If another user within your organization wishes to use the INSPECT Dataset, they must register as an individual user and comply with all the terms of this Research Use Agreement.

You must not modify, reverse engineer, decompile, or create derivative works from the INSPECT Dataset. You must not remove or alter any copyright or other proprietary notices in the INSPECT Dataset.

The INSPECT Dataset has not been reviewed or approved by the Food and Drug Administration, and is for non-clinical, Research Use Only. In no event shall data or images generated through the use of the INSPECT Dataset be used or relied upon in the diagnosis or provision of patient care.

THE INSPECT Dataset IS PROVIDED "AS IS," AND STANFORD UNIVERSITY AND ITS COLLABORATORS DO NOT MAKE ANY WARRANTY, EXPRESS OR IMPLIED, INCLUDING BUT NOT LIMITED TO WARRANTIES OF MERCHANTABILITY AND FITNESS FOR A PARTICULAR PURPOSE, NOR DO THEY ASSUME ANY LIABILITY OR RESPONSIBILITY FOR THE USE OF THIS INSPECT Dataset.

You will not make any attempt to re-identify any of the individual data subjects. Re-identification of individuals is strictly prohibited. Any re-identification of any individual data subject shall be immediately reported to the School of Medicine.

Any violation of this Research Use Agreement or other impermissible use shall be grounds for immediate termination of use of this INSPECT Dataset. In the event that the School of Medicine determines that the recipient has violated this Research Use Agreement or other impermissible use has been made, the School of Medicine may direct that the undersigned data recipient immediately return all copies of the INSPECT Dataset and retain no copies thereof even if you did not cause the violation or impermissible use.

In consideration for your agreement to the terms and conditions contained here, Stanford grants you permission to view and use the INSPECT Dataset for personal, non-commercial research. You may not otherwise copy, reproduce, retransmit, distribute, publish, commercially exploit or otherwise transfer any material.

Limitation of Use: You may use INSPECT Dataset for legal purposes only.

You agree to indemnify and hold Stanford harmless from any claims, losses or damages, including legal fees, arising out of or resulting from your use of the INSPECT Dataset or your violation or role in violation of these Terms. You agree to fully cooperate in Stanford’s defense against any such claims. These Terms shall be governed by and interpreted in accordance with the laws of California.

C.3 Data Format

We detail and define our cohort in the data using a master cohort CSV file (inspect_cohort.csv), with the following primary columns.

1. patient_id: The de-identified patient id
2. procedure_time: The date of the CTPA procedure, in ISO 8601 format
3. split: A string, either "train", "valid", or "test" that indicates the data split for this patient

The primary keys for our cohort are patient_id and procedure_time. Every case, label, and feature set is associated with a patient_id / procedure_time pair.

This file also includes the following demographic columns: age, gender, race, ethnicity.

We additionally include various columns for labels.

First, we include three NLP based pulmonary embolism diagnostic label columns. pe_positive_nlp is the main PE label used in all of our experiments and described as "Positive PE" in Appendix D.1. pe_acute_nlp and pe_subsegmentalonly_nlp are the other two label columns that are similarly described in Appendix D.1. Every case in our cohort is assigned either "True" or "False" for each of these columns.

Second, we include seven prognostic label columns. These label columns correspond to the seven prognostic tasks in our paper and have the following names: 1_month_mortality, 6_month_mortality, 12_month_mortality, 1_month_readmission, 6_month_readmission, 12_month_readmission, 12_month_PH. Every case in our cohort is assigned either "True", "False", or "Censored" for each of these columns.

Finally, we include indicators for whether or not each case in this dataset is also present in either of the RNSA or Radfusion datasets using the RSNA and radfusion columns respectively.

C.3.1 CTPA

The CTPAs are made available in DICOM format. To ensure patient privacy, patient ID and study date were anonymized, and only a subset of the DICOM headers from the original DICOM file are included: ['InstanceNumber', 'ImagePositionPatient', 'PixelSpacing', 'RescaleIntercept', 'RescaleSlope', 'WindowCenter', 'WindowWidth', 'Manufacturer', 'PhotometricInterpretation', 'SliceThickness']

C.3.2 Radiologist Report Impressions

Radiologist reports with impressions sections, after the anonymization process, are included in a CSV file with the name INSPECT_anon_impression.csv.

It contains columns with the names: PatientID, StudyTime and anon_impression, where the first two columns are used to map to the master cohort file and anon_impression is the anonymized impression section.

C.3.3 Structured EHR Data

Structured EHR data is released as gzipped CSV files in the FEMR format, which is documented at https://github.com/som-shahlab/femr/blob/main/tutorials/2b_Simple_ETL.ipynb. We release all known diagnoses, procedures, lab tests, medications, visits, and death records for patients in our cohort. The FEMR format is a simplified subset of OMOP 5.3 [57], with a subset of the columns and tables. It can be processed with any CSV reader as well as with the FEMR software package.

C.4 Dataset Statistics

C.4.1 CTPA

Based on our inclusion criteria, each CTPA study can have between 50 to 600 slices. On average, each CTPA has 220.6 slices, giving us a total of 5,164,472 CT slices in our dataset. The CTPA studies range from 1.00mm to 3.00mm (Table 7) collected from CT scanners by 3 different manufacturers (Table 8).

Slice Thickness	Count
3.00	8,600
2.50	2,840
2.00	8
1.50	5,366
1.25	7,834
1.00	16,911

Table 7: Slice Thickness Distribution

C.4.2 Structured EHR Data

Distribution of history and follow-up times Our released EHR data contains all of Stanford’s records for each patient in our cohort. As such, we have relatively substantial history before and follow-up time after each CTPA procedure in our cohort. Figure 5 provides the distributions for both the amount of history and the amount of follow-up time in days for our dataset. For the patients who

Manufacturer	Count
SIEMENS	11,357
GE MEDICAL SYSTEMS	3,786
TOSHIBA	3,072

Table 8: CT Scanner Manufacturer Distribution

	Min	Max	Average	Standard deviation
Interval (in days)	0	6887	448.19	764.87

Table 9: Statistics of CTPA scans intervals across all patients

underwent multiple CTPA scans we also calculate some basic statistics of the intervals, shown in Table 9.

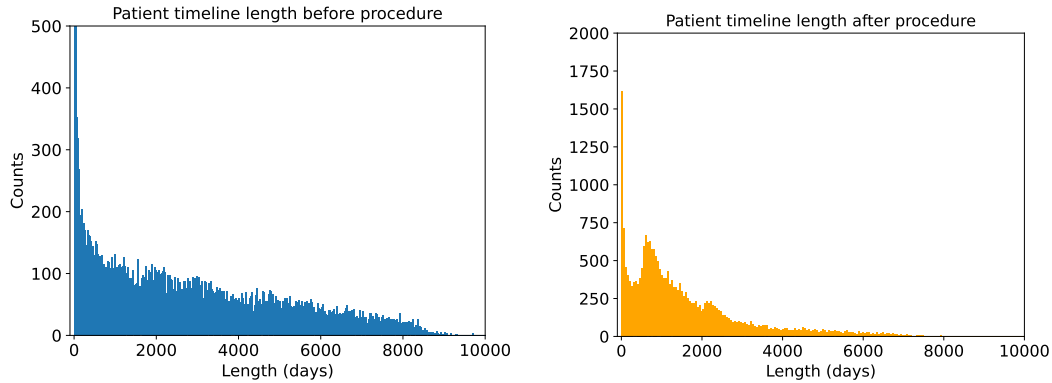


Figure 5: Patient timeline length distributions

Distribution of data types Here we show the types of data (clinical events) in the EHR patient timelines (Figure 6). We can see the measurement table dominates the OMOP table distribution and is larger than others by an order of magnitude.

C.5 Model Releases

To aid reproducibility, we release all models trained in our experiments as part of the dataset.

EHR models are in the form of pickle objects, either LightGBM Classifiers for the LightGBM models or sklearn LogisticRegression for the linear probes for MOTOR.

CT models are saved in the form of PyTorch checkpoints.

D Task Label Definitions And Validation

As part of our project, we developed and validated a set of diagnostic labels for pulmonary embolism and a set of prognostic labels for the risk of pulmonary hypertension for every case in our dataset.

D.1 Pulmonary Embolism

Task Label Definition

We construct three sets of pulmonary embolism labels ("Positive PE", "Subsegmental PE", and "Acute PE"). All the primary analysis in the benchmark is done using "Positive PE", but we release all three

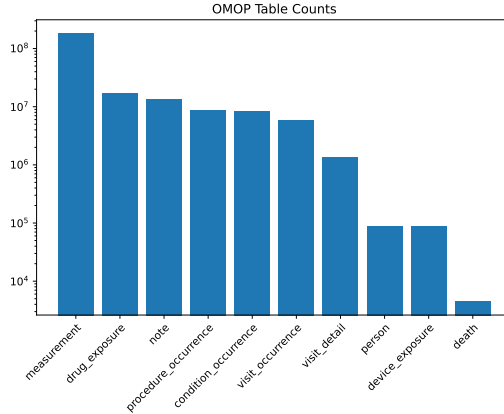


Figure 6: OMOP table distribution

as part of our dataset. We define these labels using the impression section of radiology reports as ground truth. If the radiology report contains evidence of the label, we consider that to be a positive example. If the radiology report is either unclear or contains evidence against the label, we consider that a negative. We shifted the prediction time of PE to 24 hours before the CTPA exam time to avoid feature leakage, following [30].

To develop our NLP PE labeler, we use the annotated dataset described in Banerjee et al. 2019 [5]. This dataset includes 4,351 CTPA reports obtained from Stanford Healthcare Center between 2000-2016. All reports were manually annotated by board-certified radiologists according to the following labels:

- **Positive PE:** This label is critical as it signifies the presence of a PE, a potentially life-threatening condition where one or more of the pulmonary arteries in the patient’s lungs is blocked by a blood clot. Accurate identification of PE in radiology reports is a crucial step towards timely treatment and patient recovery.
- **Subsegmental PE:** This label indicates a PE that affects the subsegmental branches of the pulmonary arteries, the smaller vessels within the lung. This label is essential in tailoring patient treatment as subsegmental PE sometimes have different treatment protocols compared to PE located in the larger pulmonary arteries. The classification of PE down to the subsegmental level is vital for precision medicine.
- **Acute PE:** This label marks a sudden onset of PE. Acute PE is particularly significant due to its immediate risk to the patient. Rapid identification and treatment of acute PE can mean the difference between life and death. As such, the Acute PE label serves as an urgent signal in the patient’s radiology report, prompting immediate medical intervention.

Using these reports and labels, we train a text-based labeling model that can automatically label the impression sections of radiology reports with "Positive PE", "Subsegmental PE", and "Acute PE" labels. We utilize a pretrained version of the Clinical Longformer model [45], as the backbone of our NLP labeler. This model is then finetuned, validated, and tested using our hand-labeled cases. After finetuning, this model is applied to generate labels for every case in our dataset, with the "Positive PE" label in particular used for all analyses. Each label was deemed positive if the model’s prediction probability exceeded 0.5; otherwise, the label was classified as negative. The labeling process is shown in Figure 7.

Task Label Validation

We validate our PE NLP labels using the test set of the manual labels. The performance of the model can be found in Table 10. The precision and recall are quite high, especially for the main "Positive PE" label, indicating that our NLP-generated labels are high quality.

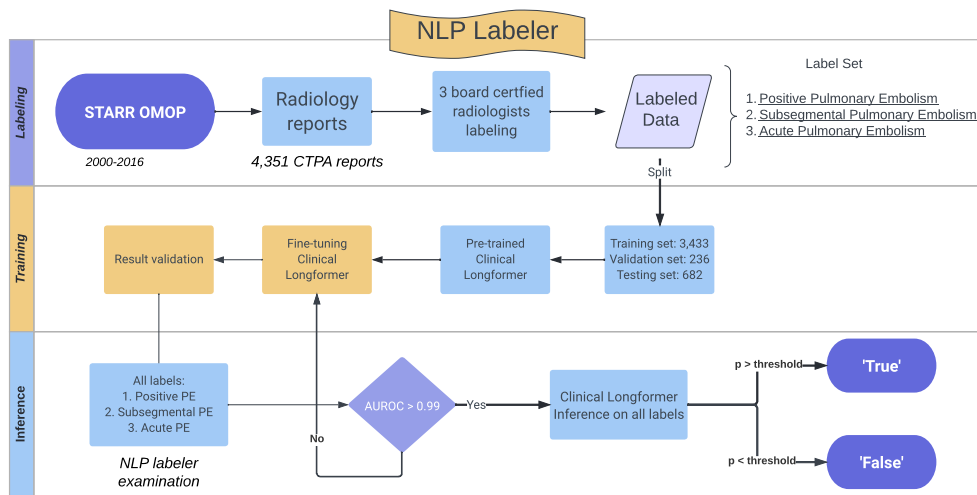


Figure 7: A flowchart of our NLP labeling process.

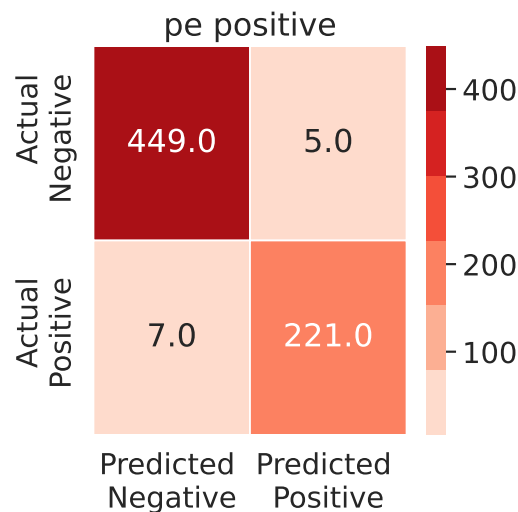


Figure 8: Confusion matrix between NLP labeler and human experts on notes under test set of our training data for NLP labeler

Even with satisfactory performance, we are interested to know the error modes of our NLP labeler so we manually examine the predictions of it against the ground truth. The confusion matrices are shown in Figure 8. When comparing against human annotation on notes, for false positive cases, we observed that the NLP might have mistakenly used the wording ‘...*thrombus within the superior vena cava...*’ as an indicator of positive pulmonary embolism when it is not. For false negative cases, the NLP labeler might have incorrectly used the wordings ‘...*possible pulmonary emboli are incompletely evaluated. Consider ct pe protocol if clinically indicated...*’ as positive PE. Overall the misclassifications when compared to experts’ annotated notes are relatively low (12 out of 682).

D.2 Pulmonary Hypertension

Task Label Definition

We construct a set of prognostic pulmonary hypertension labels that attempt to define whether or not a patient has a future incidence of pulmonary hypertension in the next year.

	Positive PE	Subsegmental PE	Acute PE
AUROC	0.99	0.99	0.99
F1	0.97	0.95	0.96
Precision	0.97	0.98	0.98
Recall	0.98	0.93	0.94
Accuracy	0.98	0.99	0.98
Class counts (pos)	228	43	201
Class counts (neg)	454	639	481
Total support	682	682	682

Table 10: NLP PE labeler performance. Each label was deemed positive if the model’s prediction probability exceeded 0.5; otherwise, the label was classified as negative.

	# Patients
Positive PH	97
Negative / Unknown PH	23

Table 11: Statistics for our ground truth hand-labeled pulmonary hypertension labels.

We start by having a board-certified clinician create a manually annotated label set for this task on 120 patients in our cohort. We define ground truth for this task based on the review of a subset of notes for those patients. Each of these notes is either labeled "Positive" or "Negative", where "Positive" is that the patient has pulmonary hypertension and "Negative" is that the patient either doesn’t have pulmonary hypertension or it is unknown. We then aggregate these labels at the patient level, labeling a patient with any "Positive" label as "Positive" and "Negative" otherwise. The statistics for these labels are in table 11.

Hand-labeling all of the cases in our dataset is not viable so we use this seed set of manual labels to develop a structured data-based phenotyping algorithm that can then be applied to all of the patients in our dataset. From manual review and expert assistance, we derive Table 12 which contains a comprehensive list of ICD and internal Stanford codes that can be used to identify pulmonary hypertension. This phenotyping algorithm is applied to obtain the pulmonary hypertension labels that we use for our primary analysis.

Task Label Validation

We validate our pulmonary hypertension phenotyping algorithm by testing it using the hand-labeled set. Our hand labels don’t incorporate time, so we can’t directly compare the 12-month PH task used in our analysis to them. Instead, we compare a slightly modified algorithm that uses the same ICD/Stanford code list to identify patients who have ever had PH and compare that set of patients to the set of "Positive" patients in our hand-labeled set. The precision, recall, F1 and accuracy are in Table 13. Our phenotyping algorithm has a very high recall, of 0.91, with slightly worse precision. The reduced precision is likely due to how we only hand labeled a subset of notes, so our ground truth here has poor recall. Regardless, this demonstrates that the structured data phenotyping algorithm we are using is effective.

E Example of CTPA scan

For the readers who are unfamiliar with CTPA, we also attached an example in Figure 9. This scan demonstrates an MPR (multi-planar reconstruction) format rendering of the 3D volumetric CTPA scan from our INSPECT cohort.

Table 12: Concepts of pulmonary hypertension and their ICD9/10 codes

Concept Name	Vocabulary ID	Code
Pulmonary hypertension	STANFORD_CONDITION	1029634
Secondary pulmonary arterial hypertension	ICD10CM	I27.21
Pulmonary hypertension due to left heart disease	ICD10CM	I27.22
Chronic pulmonary heart disease	ICD9CM	416
Kyphoscoliotic heart disease	ICD9CM	416.1
Chronic pulmonary embolism	ICD9CM	416.2
Other secondary pulmonary hypertension	ICD10	I27.2
Other secondary pulmonary hypertension	ICD10CM	I27.29
Eisenmenger's syndrome	ICD10CM	I27.83
Primary pulmonary hypertension	ICD10	I27.0
Primary pulmonary hypertension	ICD9CM	416.0
Other chronic pulmonary heart diseases	ICD9CM	416.8
Other specified pulmonary heart diseases	ICD10CM	I27.89
Chronic pulmonary embolism	ICD10CM	I27.82
Pulmonary hypertension due to alveolar hypoventilation disorder	STANFORD_CONDITION	1170535
Kyphoscoliotic heart disease	ICD10CM	I27.1
Pulmonary hypertension, unspecified	ICD10CM	I27.20
Pulmonary hypertension due to lung diseases and hypoxia	ICD10CM	I27.23
Chronic pulmonary heart disease, unspecified	ICD9CM	416.9
Cor pulmonale (chronic)	ICD10CM	I27.81
Pulmonary heart disease, unspecified	ICD10CM	I27.9
Pulmonary heart disease, unspecified	ICD10	I27.9
Primary pulmonary hypertension	ICD10CM	I27.0
Kyphoscoliotic heart disease	ICD10	I27.1
Secondary pulmonary hypertension	STANFORD_CONDITION	67294
Chronic pulmonary heart disease (CMS-HCC)	STANFORD_CONDITION	142308
Chronic thromboembolic pulmonary hypertension	ICD10CM	I27.24
Other secondary pulmonary hypertension	STANFORD_CONDITION	2065632
Other secondary pulmonary hypertension	ICD10CM	I27.2

Positive PH	
F1	0.88
Precision	0.85
Recall	0.91
Accuracy	0.80

Table 13: Structured data-based PH labeler performance.

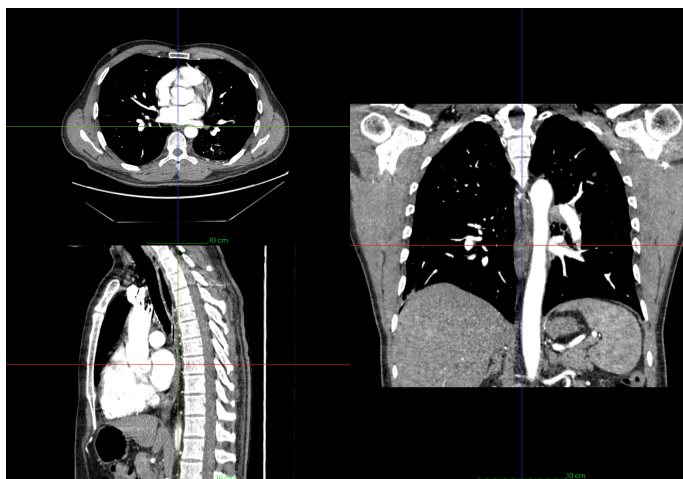


Figure 9: An example of CTPA examination scan in multi-planar reconstruction

Hyperparameters	Values
LightGBM	
max_depth	3, 6, -1
learning_rate	0.02, 0.1, 0.5
num_leaves	10, 25, 100
software_version	LightGBM 3.3.5
MOTOR	
linear_probe_l2_strength	automatic between 10 and 0
dropout	0
learning_rate	10^{-5}
num_time_bins	8
survival_dim	512
inner_dim	768
layers	12
max_sequence_length	16,384
vocabulary_size	65,536
software_version	femr 0.1.8
CTPA Slice Encoder	
learning_rate	0.0005
optimizer	AdamW
loss	BCEWithLogitsLoss
architecture	resnext101_32x8d
pretrain data	BigTransfer
software_version	timm 0.9.2
CTPA Sequence Encoder	
learning_rate	0.001, 0.0005, 0.0001, 0.00005
n_epochs	50
slice aggregation	max, mean, attention, attention+max
sequence encoder type	LSTM, GRU, Transformer
hidden size	128, 256, 512
bidirectional	True, False
num_layers	1, 3, 5
dropout_prob	0.0, 0.25, 0.5, 0.75
weighted_sampling	True, False
pretrain data	RSNA RESPECT
input_size	256
PE NLP Labeler	
max_sequence_length	1536
learning_rate	2e-5
n_epochs	15
architecture	Longformer
pretrain type	Clinical-Longformer
software_version	hugging face 4.30.1

Table 14: Hyperparameter search grids of methods under comparison in our experiments. The software version for implementing each method is also shown.

F Additional Model Details And Hyperparameters

Hyperparameters are selected through grid search on the validation set. Table 14 contains the hyperparameter grids, and the software versions used for each model.

F.1 CTPA model

Windowing We here begin to describe the viewing window for our CTPA imaging model. (window center = -600, window width = 1500), pulmonary embolism (window center = 400, window width = 1000), and the mediastinum (window center = 40, window width = 400). Specifically, for each viewing window, we clipped the Hounsfield Unit (HU) pixel values to fall within the range $[windowcenter - windowwidth/2, windowcenter + windowwidth/2]$

Slice Encoder Augmentations After the windowing operation, every CT scan is resized to dimensions of 256x256 followed by a random cropping operation to yield a 224x224 size. Before inputting into the model, each slice is normalized using the mean and standard deviation values from ImageNet. Once the slice encoder training phase is concluded, each slice is inputted into the trained model for the extraction of a latent representation. In this phase, center cropping is applied as opposed to random cropping for retrieving slice representations.

Sequence Encoder Augmentations Before the slice representations are input into a sequence encoder, we ensure each series is standardized to the same input size through either random sampling or padding. Specifically, if a series has a higher slice count than num_slices, a random sampling of the slices is conducted to equalize with num_slices. Alternatively, if a series possesses fewer slices, padding is executed with zero vectors to complete the series.

F.2 Structured Electronic Health Records Models

Gradient Boosted Tree Model

For our featurization, we use count featurization augmented by ontologies. For count featurization, we count each occurrence before the prediction time of every medical code (diagnoses, procedures, lab orders, and medications) and have a column containing the count for each code. Normally, this is a very sparse matrix as each code individually is relatively rare, so we take advantage of the standard *ontology expansion* technique, where we count higher level concepts in addition to the raw codes themselves. For instance, we will have a column both for the number of very specific ICD/I27.29 codes as well as a column for the more generic ICD/IXX (and I class ICD code) concept.

These features are then fed into a hyperparameter tuned LightGBM model [35].

MOTOR Model

MOTOR [63] is a self-supervised transformer model designed for long-term medical prediction. For our experiments, we use a version that was already pretrained on de-identified Stanford data. We explicitly construct our training, validation, and test cohorts in sync with that pretrained model such that there is no overlap between its pretraining data and our test and validation data.

We use the linear probe method for adapting MOTOR to our tasks. Aka, we extract the final patient representation from the last transformer layer and then train a logistic regression model with L2 regularization on those representations.

F.3 Model Fusion

For model fusion, we apply a simple late fusion strategy of taking a weighted average of the outputs of each source model. We implement this by first converting all output probabilities to logits, and then fitting a logistic regression model on those logits using the validation set. We do not use any regularization for that logistic regression model as it only has at most 3 features in our setup.

Furthermore, we examine the agreement and disagreement between the three source models by computing the Spearman correlations between their output probabilities on the 8 tasks in our dataset. Figure 10 contains the corresponding heatmaps. As expected, the two EHR based models, MOTOR and GBM, are much more correlated with each other than the CT based model.

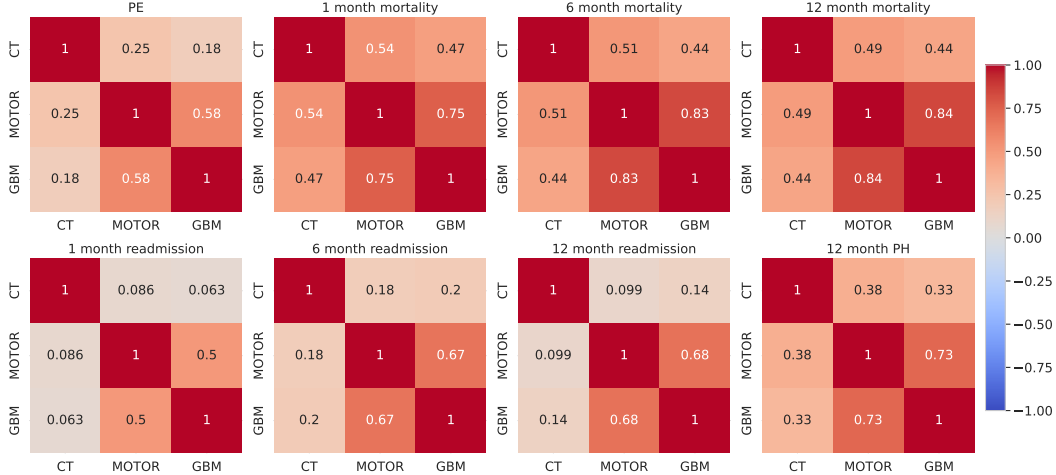


Figure 10: Spearman correlation matrices for each pair of models’ output probabilities. **CT** is the CTPA based LRCN model, **M** is the structured EHR based MOTOR model, and **G** is the structured EHR based gradient-boosted trees model.

Input Modality			Diagnostic	Prognostic						
Image	EHR		PE	In-Hospital Mortality			Re-admission			PH
CT	M	G	(+)	1 m	6 m	12 m	1 m	6 m	12 m	12 m
✓			(0.69, 0.75) (0.66, 0.70) (0.66, 0.71)	(0.76, 0.83) (0.91, 0.94) (0.82, 0.87)	(0.73, 0.78) (0.89, 0.92) (0.85, 0.88)	(0.72, 0.77) (0.88, 0.91) (0.84, 0.87)	(0.50, 0.60) (0.73, 0.81) (0.69, 0.78)	(0.48, 0.55) (0.75, 0.81) (0.71, 0.77)	(0.49, 0.56) (0.74, 0.79) (0.70, 0.75)	(0.63, 0.69) (0.80, 0.85) (0.80, 0.85)
✓	✓		(0.74, 0.78) (0.74, 0.79)	(0.91, 0.94) (0.84, 0.89)	(0.89, 0.92) (0.86, 0.89)	(0.88, 0.91) (0.85, 0.88)	(0.73, 0.82) (0.69, 0.78)	(0.75, 0.80) (0.71, 0.76)	(0.74, 0.79) (0.70, 0.75)	(0.80, 0.84) (0.81, 0.85)
✓	✓	✓	(0.68, 0.72) (0.75, 0.79)	(0.91, 0.94) (0.91, 0.94)	(0.89, 0.92) (0.89, 0.92)	(0.88, 0.91) (0.88, 0.91)	(0.74, 0.82) (0.74, 0.82)	(0.76, 0.81) (0.76, 0.81)	(0.75, 0.80) (0.75, 0.79)	(0.82, 0.87) (0.82, 0.86)

Table 15: 95% confidence intervals as a function of the test set for model performance in AUROC. **CT** is the CTPA based LRCN model, **M** is the structured EHR based MOTOR model, and **G** is the structured EHR based gradient-boosted trees model.

G Experiment Compute Environment

EHR experiments are performed in a local on-prem university compute environment using 24 Intel Xeon 2.70GHz CPU cores and 1 Nvidia V100 GPU.

Image experiments are performed on a HIPAA-compliant Google virtual machine using 4 x Nvidia V100 GPU with 96 Intel Skylake vCPU with 624GB of RAM.

All compute environments supported HIPAA-compliant data protocols.

H Confidence Intervals

We obtain some uncertainty estimates for our results by bootstrapping with respect to the test set.

First, we estimate the uncertainty of the AUROC of each model. For each task, we create 1,000 bootstrap samples and compute the AUROC for each model on each bootstrap sample. We then extract the 2.5% and 97.5% percentiles of the 1,000 samples to obtain 95% confidence intervals.

Table 15 presents the results of this analysis. The widths of the intervals are often around 0.04, indicating that we are able to estimate model performance with reasonable precision.

Second, we estimate the uncertainty of the relative AUROC of each model. We use the same bootstrap samples as in the first analysis, but compute the relative performance between each model and our chosen baseline, which we arbitrarily choose as MOTOR.

Input Modality			Diagnostic	Prognostic						
Image	EHR		PE	In-Hospital Mortality			Re-admission			PH
CT	M	G	(+)	1 m	6 m	12 m	1 m	6 m	12 m	12 m
✓			(0.01, 0.07) (0.00, 0.00)	(-0.16, -0.10) (0.00, 0.00)	(-0.17, -0.12) (0.00, 0.00)	(-0.17, -0.12) (0.00, 0.00)	(-0.29, -0.16) (0.00, 0.00)	(-0.30, -0.22) (0.00, 0.00)	(-0.28, -0.20) (0.00, 0.00)	(-0.19, -0.13) (0.00, 0.00)
	✓		(-0.02, 0.03)	(-0.10, -0.05)	(-0.05, -0.02)	(-0.05, -0.02)	(-0.08, 0.01)	(-0.06, -0.02)	(-0.06, -0.02)	(-0.02, 0.03)
	✓	✓	(0.06, 0.10)	(-0.00, 0.01)	(-0.00, 0.01)	(-0.00, 0.01)	(-0.00, 0.00)	(-0.00, 0.00)	(-0.01, 0.00)	(-0.01, 0.00)
	✓	✓	(0.06, 0.11)	(-0.08, -0.03)	(-0.04, -0.01)	(-0.04, -0.01)	(-0.08, 0.01)	(-0.07, -0.02)	(-0.07, -0.02)	(-0.01, 0.03)
		✓	(0.01, 0.03)	(-0.00, 0.00)	(-0.00, 0.00)	(-0.00, 0.00)	(-0.00, 0.02)	(0.00, 0.01)	(0.00, 0.01)	(0.01, 0.04)
	✓	✓	(0.07, 0.11)	(-0.00, 0.01)	(-0.00, 0.01)	(-0.00, 0.01)	(-0.00, 0.02)	(0.00, 0.01)	(-0.00, 0.01)	(0.00, 0.04)

Table 16: 95% confidence intervals for the difference in AUROC performance between a particular model and the structured EHR based MOTOR model. **CT** is the CTPA based LRCN model, **M** is the structured EHR based MOTOR model, and **G** is the structured EHR based gradient-boosted trees model. Statistically significant differences at $p = 0.05$ are **bolded**.

Input Modality			Diagnostic	Prognostic						
Image	EHR		PE	In-Hospital Mortality			Re-admission			PH
CT	M	G	(+)	1 m	6 m	12 m	1 m	6 m	12 m	12 m
✓			0.715, (0.003)	0.741, (0.007)	0.753, (0.001)	0.750, (0.003)	0.549, (0.008)	0.547, (0.014)	0.551, (0.012)	0.658, (0.005)

Table 17: The mean and standard deviation in AUROC for the various tasks when the random seed is changed. We use 5 random seeds to estimate both the mean and standard deviation.

Table 16 contains these relative confidence intervals. Most (12/14) of the intervals for individual models exclude zero, indicating that we have enough precision to accurately tell the difference in performance between CT, MOTOR, and gradient-boosted tree models. The fused models have a less clear separation, with about half of the differences being statistically insignificant.

In order to conduct variation study, we have rerun our image-based modality for 5 times for different seeds. Note that our EHR baselines, MOTOR and LightGBM, are deterministic with the hyperparameters we used in our study, so we do not perform reseeding experiments. The results of this analysis are in Table 17.

I Model Performance as a Function of PE Status

In our results section, we present performance statistics on the entire cohort. However, it is sometimes useful to look at performance within patients who test positive for PE (+) vs patients who test negative for PE (-). Table 18 contains the performance on the seven prognostic tasks by PE status.

J Comparison of Models vs. Simplified PESI

Clinical risk scores are heuristics commonly used in medicine to inform treatment decisions. We compare our machine learning-based models against a common PE rule-based risk calculator, the simplified PESI (sPESI) score [55]. sPESI is a 0-6 scoring rule comprised of the following additive criteria (each rule contributes +1 to the overall score) in Table 19.

To ensure that the features used to calculate sPESI reflect the patient’s condition at the time of the imaging, we only use data between the most recent 10 days prior to the CT exam and the 2 days after the CT scan for the numeric sPESI features. Patients that are missing data required for sPESI are dropped. In addition, as sPESI is only designed for use with patients that have PE, we further restrict this analysis to patients that have a positive diagnosis for PE. This results in a total of 1,719 cases derived from 1,609 unique patients with the required sPESI features and PE. The amount of patients with each total score is listed in Table 20.

We evaluate the sPESI score by measuring the performance in terms of AUROC of using the score to rank patients for our seven prognostic tasks. Table 21 contains the results of this comparison. Note that sPESI is designed for short-term mortality prediction, and might not be meaningful in the context of other prognostic tasks. We observe relatively low performance for the sPESI. One potential cause of that low performance is that our retrospective data has a much higher degree of missingness

Has PE	Input Modality			Prognostic									
	Image	EHR		In-Hospital Mortality			Re-admission			PH			
	CT	M	G	1 m	6 m	12 m	1 m	6 m	12 m	12 m			
(+)	✓	✓	✓	0.761	0.738	0.726	0.609	0.586	0.629	0.596			
				<u>0.914</u>	<u>0.897</u>	<u>0.869</u>	<u>0.782</u>	<u>0.770</u>	<u>0.755</u>	0.761			
				0.853	0.850	0.835	0.773	0.763	0.729	<u>0.762</u>			
	✓	✓	✓	0.879	0.902	0.870	0.752	0.766	0.760	0.740			
				0.817	0.858	0.844	0.712	0.748	0.732	0.740			
				0.914	0.897	0.871	0.788	0.789	0.757	0.772			
	✓	✓	✓	0.879	0.899	0.870	0.762	0.776	0.758	0.752			
				✓	✓	✓	0.806	0.758	0.754	0.534	0.504	0.507	0.677
							<u>0.925</u>	<u>0.902</u>	<u>0.897</u>	<u>0.771</u>	<u>0.782</u>	<u>0.770</u>	<u>0.852</u>
0.847	0.869	0.861	0.728				0.737	0.728	0.852				
(-)	✓	✓	✓	0.927	0.903	0.900	0.771	0.778	0.764	0.850			
				0.872	0.879	0.873	0.729	0.728	0.716	0.859			
	✓	✓	✓	0.924	0.905	0.898	0.775	0.787	0.775	0.871			
				0.926	0.905	0.901	0.775	0.783	0.768	0.868			

Table 18: The performance in AUROC for our different baseline modeling strategies, split by PE status. **CT** is the CTPA based LRCN model, **M** is the structured EHR based MOTOR model, and **G** is the structured EHR based gradient-boosted trees model. The best overall models are **bolded** and the best individual models are underlined.

#	PESI Score criteria
1	Age > 80
2	History of Cancer
3	History of Chronic Cardiopulmonary Disease
4	Heart Rate (bpm) \geq 110
5	Systolic BP (mmHg) < 100
6	O ₂ Saturation < 90%

Table 19: Criteria for PESI score

sPESI Score	# Cases With Score
0	169
1	361
2	529
3	450
4	184
5	30
6	1

Table 20: The statistics for the sPESI scores on the 1,719 cases in our cohort that it can be calculated on.

Input Modality				Prognostic						
Image	EHR			In-Hospital Mortality			Re-admission			PH
CT	M	G	P	1 m	6 m	12 m	1 m	6 m	12 m	12 m
✓				0.676	0.634	0.663	0.643	0.478	0.631	0.579
	✓			0.808	0.813	0.787	0.745	0.684	0.678	0.725
		✓		0.749	0.749	0.741	0.679	0.620	0.619	0.688
			✓	0.569	0.571	0.571	0.701	0.679	0.614	0.567

Table 21: The performance in AUROC for our different baseline modeling strategies given patients with PE. Note that this set of evaluations is only done on the subset of cases that have both PE and enough data for the simplified PESI risk score. **CT** is the CTPA based LRCN model, **M** is the structured EHR based MOTOR model, **G** is the structured EHR based gradient-boosted trees model, and **P** is the simplified PESI risk score. The best models are **bolded**.

than the prospective studies used to generate and validate sPESI. For example, our ability to extract features like the history of Chronic Cardiopulmonary Disease is relatively limited as we are restricted to structured data already within the health record.

K Additional Metrics

For our main analysis, we compare models in terms of AUROC as it is a low variance and widely used metric. However, additional metrics, especially in the clinical space, can also be important when evaluating the utility of models.

Input Modality			Diagnostic	Prognostic						
Image	EHR		PE	In-Hospital Mortality			Re-admission			PH
CT	M	G	(+)	1 m	6 m	12 m	1 m	6 m	12 m	12 m
✓			<u>0.463</u>	0.189	0.288	0.324	0.056	0.124	0.169	0.230
	✓		0.327	<u>0.396</u>	<u>0.537</u>	<u>0.588</u>	<u>0.160</u>	<u>0.342</u>	<u>0.402</u>	0.485
		✓	0.335	0.234	0.426	0.497	0.145	0.276	0.334	<u>0.582</u>
✓	✓		0.510	0.426	0.545	0.599	0.164	0.337	0.393	0.481
✓		✓	0.515	0.295	0.447	0.521	0.145	0.271	0.330	0.573
	✓	✓	0.354	0.399	0.542	0.587	0.179	0.346	0.407	0.597
✓	✓	✓	0.523	0.428	0.542	0.598	0.180	0.343	0.399	0.589

Table 22: The performance in AUPRC for our different baseline modeling strategies, including late fusion. **CT** is the CTPA based LRCN model, **M** is the structured EHR based MOTOR model, and **G** is the structured EHR based gradient-boosted trees model. The best overall models are **bolded** and the best individual models are underlined.

We thus perform additional analysis to compare our models in terms of both AUPRC (area under the precision-recall curve) (see Table 22 and ECE (expected calibration error) (see Table 23). AUPRC provides an estimate of the precision of a model under various recall thresholds and ECE provides an estimate of the calibration of a model. We use 10 bins for our ECE estimate.

The relative model performance rankings for both of these additional metrics are very similar to the rankings seen with AUROC, with the EHR models doing better at prognostic tasks while the image models do better at the diagnostic task.

Input Modality			Diagnostic	Prognostic						
Image	EHR		PE	In-Hospital Mortality			Re-admission			PH
CT	M	G	(+)	1 m	6 m	12 m	1 m	6 m	12 m	12 m
✓			0.278	0.423	0.369	0.265	0.136	0.347	0.346	0.325
	✓		0.026	<u>0.011</u>	<u>0.010</u>	<u>0.015</u>	<u>0.008</u>	0.004	0.007	<u>0.012</u>
		✓	<u>0.015</u>	0.020	0.053	0.017	0.016	0.016	0.026	0.021
✓	✓		0.024	0.004	0.012	0.017	0.009	0.009	0.010	0.016
✓		✓	0.015	0.007	0.019	0.017	0.004	0.009	0.014	0.023
	✓	✓	0.007	0.004	0.010	0.014	0.006	0.009	0.014	0.009
✓	✓	✓	0.016	0.005	0.011	0.015	0.006	0.009	0.013	0.025

Table 23: The calibration performance in ECE for our different baseline modeling strategies, including late fusion. Lower scores indicate better models with this metric. **CT** is the CTPA based LRCN model, **M** is the structured EHR based MOTOR model, and **G** is the structured EHR based gradient-boosted trees model. The best overall models are **bolded** and the best individual models are underlined.